Chair of Scientific Computing
Department of Computer Science
Technical University of Munich

TUM

Master Thesis

Creating a Quantum Analogue to an Arbitrary Classical Elementary Cellular Automaton

Benjamin Decker

TUM Uhrenturm

Master Thesis

Creating a Quantum Analogue to an Arbitrary Classical Elementary Cellular Automaton

Benjamin Decker

Chair of Scientific Computing
Department of Computer Science
Technical University of Munich

TUT

Master Thesis

Creating a Quantum Analogue to an Arbitrary Classical Elementary Cellular Automaton

Benjamin Decker

Thesis for the attainment of the academic degree

Master of Science (M.Sc.)

at the Department of Computer Science of the Technical University of Munich.

Examiner:
Prof. Dr. Christian Mendl

Supervisor:
Richard Milbradt

Submitted:
Munich, 08.10.2024

I hereby declare that this thesis is entirely the result of my own work except where otherwise indicated. I have only used the resources given in the list of references.

Munich, 08.10.2024   Benjamin Decker

Abstract

There have been approaches to finding quantum cellular automata inspired by elementary cellular automata in the past [Ney+22; BCM12]. However, a method to create a quantum analogue for arbitrary elementary cellular automata is still missing.

The Wolfram code is a system for labeling all 256 classical elementary cellular automata [Wol83]. This thesis presents a method to create a classically inspired quantum analogue for each elementary cellular automaton, in the form of a 1-dimensional spin-$\frac{1}{2}$ chain governed by a sum of local Hamiltonians.

Quantum analogues to non-reversible classical CAs are presented as non-unitary quantum systems governed by non-hermitian Hamiltonians. Two possible sets of non-hermitian operators for governing such evolutions are presented and analyzed.

The resulting quantum systems are analyzed and compared to their classical counterparts for selected rules. Similarities include convergence to a similar state, and showing the same behavior in static and periodic cases. Known quantum phenomena like ergodicity and its breaking due to Hilbert space fragmentation are identified and explained for selected systems, where parallels to well-studied systems like the PXP-model are drawn.

Acknowledgements

First and foremost, I want to thank my Thesis supervisor Richard Milbradt. He accompanied me through no less than 4 projects since the beginning of my Master's studies, culminating in this thesis. From talking to my fellow students, I know how hard it can be to find a research area that fits ones interests while also convincing possible advisors to collaborate on projects or theses in those fields. I am therefore grateful to Richard for not only helping me to find topics for my projects, which is not something to be taken for granted, but also being an invaluable source of knowledge when I needed help or got stuck.

I also want to thank Prof. Dr. Christian Mendl, whose lectures were among the ones I enjoyed during my Master's, introducing me to the field of quantum computing. It was one of the seminars organized by Christian where I began writing the code that I now made heavy use of for this thesis and will keep maintaining into the future. Despite his busy schedule, he remained approachable and open to questions and personal meetings, even going so far as to offer me to call him Christian.

Lastly, I am grateful to my friends and family, who gave general writing advice and kept me motivated by joining studying/writing sessions, often lasting late into the night.

Contents

1 Introduction

Stephen Wolfram, one of the most prominent researchers in the field of cellular automata (CAs) [WW17; Wol18] and inventor of the Wolfram Code for elementary CAs [Wol83], wrote in one of his papers "Cellular automata are sufficiently simple to allow detailed mathematical analysis, yet sufficiently complex to exhibit a wide variety of complicated phenomena." [Wol83]. Wolframs sentiment also holds true for quantum cellular automata (QCAs) (cf. Chapter 3). This unexpected similarity warrants searching for further connections between classical and quantum CAs, as a lot of research has gone into understanding classical CAs [Wol83; Coo04; LP+90], so there is hope that shedding a light on the similarities between classical and quantum CAs might let us leverage known results to improve our understanding of quantum systems.

As this thesis shows, despite classical and quantum systems being completely different in general, with some work, there is a way to create quantum analogues to a classical elementary CAs, governed by an arbitrary rule from the Wolfram code. As it turns out, when viewing these systems side by side, they often show a surprising amount of similarity (cf. Section 4.1), ranging from time evolutions that look completely identical (cf. Section 4.1.1), over similar convergence behaviors (cf. Section 4.1.2), to similar periodic-seeming behaviors (cf. Section 4.1.3).

However, not all rules produce similar time evolutions for the classical and quantum cases (cf. Section 4.2). Despite this, these systems often bridge a gap to well-studied quantum systems like the PXP-model [Tur+18; IV20] (cf. Section 4.2.3). This connection enables comparing the PXP-model to a set of other rules with an identical time evolution when confined to a specific subspace. Results like this reinforce the above-mentioned idea that an intuitive understanding of quantum systems can be gained from analyzing classically motivated quantum systems.

2 Classical Cellular Automata

2.1 Definitions

The following is a summary of terms used to classify CAs in this thesis. Given a CA defined by a grid of cells G, a rule R, and an initial state:

Dimension The number of spacial dimensions D of the cell grid

Grid of Cells $G \subset \mathbb{Z}^D$ where each cell is identified by a D-tuple

Local Dimension The number of possible states d a cell can be in

Distance $\Delta\left(\vec{x}, \vec{y}\right) = \max_{i \in \{1,\dots,d\}} \left(|x_i - y_i|\right)$ where $\vec{x}, \vec{y} \in G$
   The Chebyshev distance (L_∞ metric) on the cell grid

Support $\sup\left(\vec{x}\right) \subseteq R$ where $\vec{x} \in G$
   The set of cells that has to be taken into account when mapping a cell state to its state in the next time step

Rule $R : \sup\left(\vec{x}\right) \longrightarrow \{1\dots, d\}$
   A mapping from cell support to cell state

Range $r(R) = \max\left\{\Delta\left(\vec{x}, \vec{y}\right) | \vec{x}, \vec{y} \in \sup(R)\right\}$
   Maximum among distances from a cell to cells in its support

Neighborhood $N\left(\vec{x}\right) = \left\{\sup\left(\vec{x}\right) \setminus \{\vec{x}\}\right\}$
   The support of a cell minus the cell itself

A CA consists of a regular grid in an arbitrary dimension, a finite amount of states each grid point can be in, and a rule that determines if and how the state of a grid point changes depending on its current state and the states of its neighbor cells. Given an initial state of the grid, the automaton can then be simulated step by step, often displaying unexpectedly complex behavior.

One of the best-known examples of a classical CA is Conway's Game of Life, a CA with $D = 2, d = 2$ and a range of 1, named after its discoverer John Horton Conway in 1970 [ICS15]. The two possible grid states
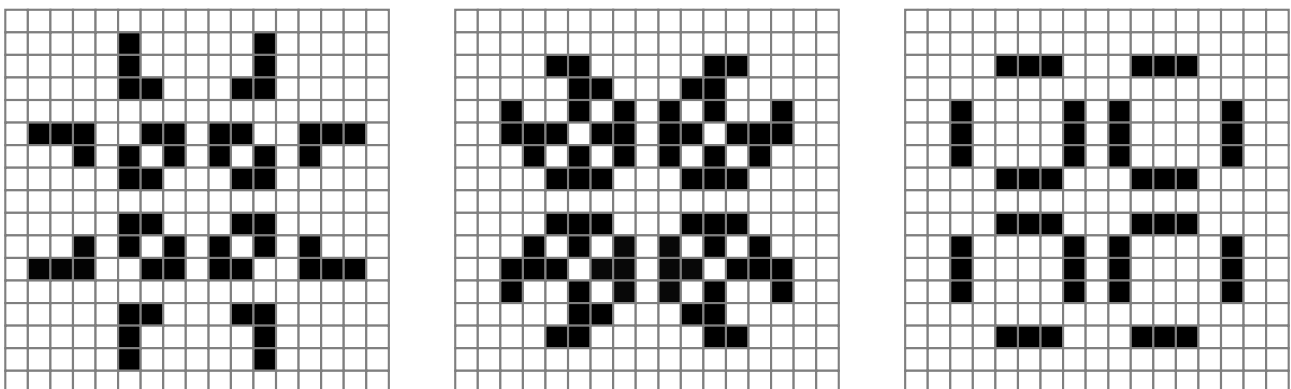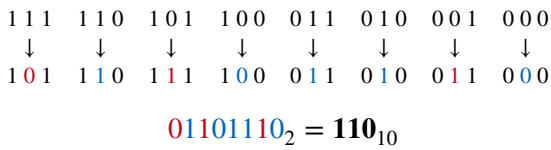

Figure 2.1 All 3 states of a pulsar with period 3 in Conway's Game of Life. A state changes to the one on its right after one time step, after 3 steps, the pattern repeats itself.

$$111 \quad 110 \quad 101 \quad 100 \quad 011 \quad 010 \quad 001 \quad 000$$
$$\downarrow \qquad \downarrow \qquad \downarrow \qquad \downarrow \qquad \downarrow \qquad \downarrow \qquad \downarrow \qquad \downarrow$$
$$101 \quad 110 \quad 111 \quad 100 \quad 011 \quad 010 \quad 011 \quad 000$$

$$01101110_2 = \mathbf{110}_{10}$$

(a) The top row shows each possible state triplet of adjacent cells in order of descending numerical value. The bottom row shows the triplets after applying some mapping. Red bits indicate a flip, blue bits remain unchanged. The rule code is defined by interpreting the red and blue bits as a binary number.
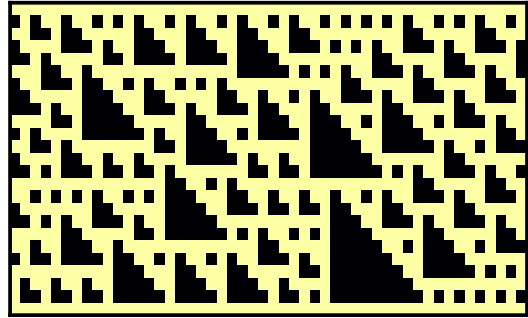
(b) The time evolution of the Rule-110 automaton with a random initial state and open boundary conditions. Time is plotted on the x-axis, space on the y-axis.

Figure 2.2 The Rule-110 elementary cellular automaton

are often called "alive" and "dead", inspired by the analogy of cells dying or coming alive due to under- or overpopulation in their immediate neighborhood.

There are a lot of known initial states in the Game of Life with predictable behavior, like the "pulsar" with a period of 3 time steps shown in Figure 2.1. The pulsar is predictable in the sense that its form is known form any possible point in the future. However, for random initial states, the time evolution of a CA generally does not converge to static or periodic behavior and is therefore not easily predictable [Wol18]. In fact, for some configurations, to find out how they will have changed after n time steps or whether or not their evolution will end up in a static or periodic configuration, there is no faster way than to simulate the CA for n time steps [BCG04]. This hints to a close relation to the halting problem, supported by the fact that the Game of Life is computationally universal [BCG04].

While this result is surprising, as it turns out, there exists an even simpler class of CA also fulfilling universality: Elementary CAs [Coo04].

2.2 Elementary CAs & The Wolfram Code

The properties of all further CAs considered in this thesis are $D = 1, d = 2$ with a range of 1. Such CAs are called elementary [Wol83]. Despite their relative simplicity, having the lowest possible sensible dimension and range, they can show surprising complexity and are even proven to be Turing complete [Sut09].

The rule of an elementary CA is defined by how the state of a cell changes from one time step to the next, depending on its own state and the states of its direct neighbors. In other words, a rule is a mapping from cell state triplets representing the cell and its neighbors, to single-cell states representing the state after one time step. Since the number of all such possible mappings is finite and relatively small, an efficient naming scheme, the Wolfram Code, can be used to label them.

First introduced in 1983 [Wol83], the Wolfram Code of an elementary cellular automaton is a number from 0 to 255, labeling its rule and encoding its mapping. The mapping is encoded in the digits of the binary representation of the rule, where each digit corresponds to one of the $2^3 = 8$ possible binary cell triplets and controls whether or not the center cell of a triplet is mapped to 0 or 1. Figure 2.2a illustrates this process for the Rule-110 automaton. Figure 2.2b shows the CA's time evolution, following this rule from a random initial state, where a surprisingly complex pattern emerges.

For the purpose of analyzing Wolfram rules, and especially for implementing a quantum CAs from them (cf. Chapter 3), it can be useful to classify the behavior of a cell only in a specific neighborhood, leading to the concept of neighborhood rule tuples (NRTs).

b	1□1		1□0		0□1		0□0	
time step	1 1 1 ↓ 1 0 1	1 0 1 ↓ 1 1 1	1 1 0 ↓ 1 1 0	1 0 0 ↓ 1 0 0	0 1 1 ↓ 0 1 1	0 0 1 ↓ 0 1 1	0 1 0 ↓ 0 1 0	0 0 0 ↓ 0 0 0
NRT(110, b)	(0, 1)		(1, 0)		(1, 1)		(1, 0)	
behavior	bit flip		no change		set to 1		no change	
type	reversible		reversible		peripheral		reversible	

(a) Rule 110

b	1□1		1□0		0□1		0□0	
time step	1 1 1 ↓ 1 1 1	1 0 1 ↓ 1 0 1	1 1 0 ↓ 1 0 0	1 0 0 ↓ 1 1 0	0 1 1 ↓ 0 0 1	0 0 1 ↓ 0 1 1	0 1 0 ↓ 0 1 0	0 0 0 ↓ 0 0 0
NRT(150, b)	(1, 0)		(0, 1)		(0, 1)		(1, 0)	
behavior	no change		bit flip		bit flip		no change	
type	reversible		reversible		reversible		reversible	

(b) Rule 150

Figure 2.3 NRT-decompositions for rules 110 and 150 of the Wolfram code. The change of a cell c, labeled with the placeholder □, depending on its neighborhood b is shown. The state of c after applying the rule, depending on its previous state, is encoded in an NRT-tuple. Each NRT can be classified as reversible or peripheral, according to Table (2.2)

2.2.1 Neighborhood Rule Tuples

By applying a rule r to a cell with state s_{before} and its neighborhood b, the cell's state will either flip or stay the same, resulting in s_{after}. Doing so for both possible initial states 0_{before} and 1_{before}, and labeling the respective resulting states 0_{after} and 1_{after}, results in a NRT for r and b:

$$\text{NRT}(r, b) = \left(1_{\text{after}}, 0_{\text{after}}\right) \tag{2.1}$$

A NRT describes how a cell state changes for a fixed environment, depending on its initial state. Given the possibilities for 1_{after} and 0_{after}, there are $2^2 = 4$ possible NRTs, each with a unique behavior and belonging to one of 2 types:

NRT(r, b)	(0, 0)	(0, 1)	(1, 0)	(1, 1)
behavior	set to 0	bit flip	no change	set to 1
type	peripheral	reversible	reversible	peripheral

(2.2)

Reversible NRTs describe actions where no information about the previous state of a cell is lost, making them reversible. In contrast, the term peripheral describes the opposite. First introduced in [Wol83], it describes an elementary CA rule in which "the value of a particular site depends on the values of its two neighbors at the previous time step, but not on its own previous value." By extension, in a peripheral NRT the resulting cell state only depends on the neighborhood, not on the previous state of the cell itself. All information about the previous cell state is lost, making the action described by a peripheral NRT non-reversible.

Since rules can be thought of as consisting of a collection of NRTs, these classifications can also be applied to complete rules.

2.2.2 Reversible & Peripheral Rules

A rule describes the action of a cell for an arbitrary neighborhood. Thus, each rule can be decomposed into NRTs, one for each possible neighborhood. For 2 possible neighbors, each being in one of 2 possible states

respectively, this results in $2^2 = 4$ NRTs neighborhoods to consider. With 4 possible variants for each NRT (cf. Table (2.2)), this results in $4^4 = 256$ possible rules, covering every elementary CA rule from the Wolfram code.

A rule is then called reversible if its NRT-decomposition only consists of reversible NRTs and peripheral if it only consists of peripheral NRTs. There are 2 reversible behaviors and 2 peripheral behaviors among all possible NRTs, reducing the number of possible reversible or peripheral rules to $2^4 = 16$, respectively. Thus, the majority of rules are neither reversible nor peripheral, consisting of NRTs of both types.

Figure 2.3 shows NRT-decompositions for rule 150, and for the aforementioned rule 110. Rule 150 only consists of reversible NRTs and is therefore reversible, rule 110 consists of both reversible and peripheral NRTs and is therefore neither.

The Wolfram code, elementary cellular automata rules, and NRT-decompositions are descriptions of purely classical systems. However, a good understanding of those concepts will prove invaluable when creating a quantum analogue to a classical elementary CA, where NRTs will be instrumental in building a large system, from local subsystems governed by the behavior if NRTs. With that, everything is set to introduce elementary quantum cellular automata and to explore their similarity to their classical counterparts, or missing thereof.

3 Elementary Quantum Cellular Automata

QCAs are a class of quantum systems that are most often defined as a grid in D dimensions of d-dimensional quantum systems, governed by a time evolution that is translation-invariant, causal, and unitary [SW04; Arr19; Far20; Gro+12]. Such systems are of particular interest for the subject of quantum computing, as some classes of QCAs can efficiently simulate quantum Turing machines [Wat95]. Similar to the classical case, a QCA can show complex behavior arising despite it's constrained nature (Section 3.5).

Given that QCAs can be thought of as the quantum analogue of classical CAs, further similarities between the two can be explored. For instance, the Wolfram Code is a purely classical concept, but with some work, one can find ways to also apply the concept to quantum systems.

However, the similarities of classical and quantum CAs only become visible once some conventions are followed. At first glance, a QCA is rather unlike its classical counterpart, as it consists of a wave function in some high-dimensional Hilbert space, instead of single bits for each cell. Comparisons of the evolution of their respective cell states can only be made once it is clear what the state of a quantum cell is and how to perform a time evolution.

As the goal of this thesis is to form and explore a connection between purely elementary CAs and QCAs, all systems are restricted to be 1-dimensional where the local state space of each cell is 2-dimensional, to most closely resemble their classical counterparts. Additionally, in order to create a quantum analogue to an arbitrary elementary CA, the need for time evolutions to be unitary needs to be relaxed for some rules (Section 3.4).

3.1 Quantum State

The most prevalent naming scheme for classical cell states in 2 local dimensions is $\{dead, alive\}$ or $\{0, 1\}$. Thus, an obvious choice for the local basis of a QCA is the spin-$\frac{1}{2}$ basis labeled $\{|0\rangle, |1\rangle\}$, the Qubit [NC10].

By following some basic rules for constructing quantum states and measuring them, translating a classical state into a quantum wave function becomes relatively simple [NC10]: Given some classical state written as a bitstring with length equal to the number of cells, a corresponding quantum state $|\psi\rangle$ can be labeled by the same bitstring and be constructed from its local basis states:

$$
\begin{aligned}
000101000 &\longrightarrow |000101000\rangle \\
&\Longrightarrow |\psi\rangle = |0\rangle^{\otimes 3} \otimes |1\rangle \otimes |0\rangle \otimes |1\rangle \otimes |0\rangle^{\otimes 3}
\end{aligned}
\tag{3.1}
$$

where $\otimes$ is the Kronecker product. By construction, $|\psi\rangle \in \mathbb{C}^{2^9} = \mathbb{C}^{512}$. In general, the dimension of the Hilbert space scales exponentially with the number of cells l:

$$
|\psi\rangle \in \mathbb{C}^{2^l}
\tag{3.2}
$$

In contrast to the classical case where each cell is in one of 2 states at all times, the state of a quantum cell can only be given as a probability for it to be in state $|0\rangle$ or $|1\rangle$ when measured, and has to be calculated from the wave function of the whole system. The corresponding observables for a measurement at site index j are projectors onto the respective basis states at that site:

$$
n_j^{|0\rangle} = |0\rangle_j \langle 0| \qquad n_j^{|1\rangle} = |1\rangle_j \langle 1|
\tag{3.3}
$$

$$
Pr(dead)_j = \langle \psi | n_j^{|0\rangle} |\psi\rangle \qquad Pr(alive)_j = \langle \psi | n_j^{|1\rangle} |\psi\rangle
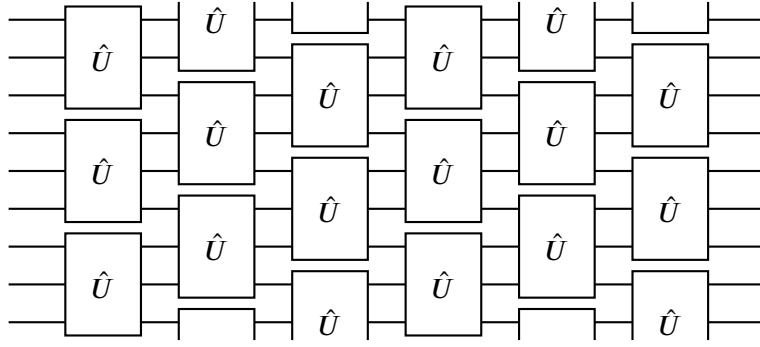\tag{3.4}
$$

Figure 3.1 A partitioned quantum cellular automaton (PQCA), represented as a quantum circuit where each wire represents one cell. The unitary operator $\hat{U}$ which governs the local time evolution on a neighborhood is applied repeatedly in an interleaving pattern.

3.2 Time Evolution

All QCAs discussed in this thesis are systems undergoing evolutions in continuous time governed by a Hamiltonian H according to the Schrödinger equation [NC10]

$$\hat{U} = e^{-it\hat{H}} \tag{3.5}$$

where the Hamiltonian is made up of a sum of identical local terms and takes the form

$$\hat{H} = \sum_i \hat{H}_j \tag{3.6}$$

While such systems are not always counted among the class of QCAs [Far20], I would argue that the following derivation as well as the fact that such systems can be simulated by more conventional QCAs [Arr19] warrants calling them QCA:

A PQCA is a QCA formed from a given interaction term $\hat{U}$ in a repeating pattern, as shown in Figure 3.1 [Arr19]. The operator $\hat{U}$ remains the same, regardless of which cells it is positioned on, thus realizing translational invariance. After each layer, information can travel at most 2 cells, ensuring causality. If additionally, $\hat{U}$ is unitary, all necessary QCA-definitions mentioned in the beginning of Chapter 3 are met. All time evolution operators $\hat{U}$ considered in this thesis are of the form given in Equation (3.5), which means that integrating Figure 3.1 over ever smaller time steps Δt results in a TEBD scheme, equivalent to a time evolution governed by a Hamiltonian made of local sums in continuous time [Pae+19; Arr19]. Thus, if all those rules are followed, which is the case for all reversible QCAs discussed in this thesis, the resulting time evolution can be simulated by a QCA. The QCA only turns into an actual evolution in continuous time in the limit of $\Delta t \to 0$. However, I admit that an even more problematic deviation from the common definition is represented by non-unitary time evolutions (Section 3.4).

The form of the Hamiltonian as it is shown in Equation (3.6) is therefore implied by the translational invariance and the identical U-operators in Figure 3.1, where each term identical term control the behavior of one neighborhood. Notice that $i \neq j$ in Equation (3.6). The problem of finding a Hamiltonian $\hat{H}$ therefore reduces to finding one local operator $\hat{H}_j$, which is then applied at all cell indices. These operators should be chosen in a way that the time evolution governed by them according to Equation (3.5) leads to the desired behavior.

The complete time evolution is then again given by the Schrödinger equation, this time governed by the complete Hamiltonian. Even though the time evolution is in continuous time, measurements are taken at discrete time steps, to resemble a classical CA in discrete space and time.

As each cell should change or stay constant, only depending on the state of itself and its nearest neighbors, a local Hamiltonian governing an equivalent dynamic on a neighborhood of quantum cells with the center cell at index j can be a written as

$$\hat{H}_j = \hat{S}_j \hat{P}_j, \tag{3.7}$$

which is a generalization of what is shown in [Ney+22]. $\hat{S}_j$ is the operator that governs the evolution of the cell at index j. $\hat{P}_j$ takes the role of an activator and is chosen to be non-zero over the set of states where the cell at index j needs to change and, zero otherwise.

A connection can be made between the operators $\hat{S}_j$ and $\hat{P}_j$ and the NRT-decomposition of a Wolfram rule (cf. Section 2.2.1), where $\hat{S}_j$ is given by the NRT-behaviors and $\hat{P}_j$ is given by the neighborhoods b. $\hat{P}_j$ is constructed as a sum of terms, one for each combination of dead or alive neighbors. There are 4 possible terms, consisting of operators from Equation (3.3), that can be included in $\hat{P}_j$, one for each NRT-neighborhood b:

Neighborhood	$0 \,\square\, 0$	$0 \,\square\, 1$	$1 \,\square\, 0$	$1 \,\square\, 1$
Term	$n_{j-1}^{\lvert 0\rangle} n_{j+1}^{\lvert 0\rangle}$	$n_{j-1}^{\lvert 0\rangle} n_{j+1}^{\lvert 1\rangle}$	$n_{j-1}^{\lvert 1\rangle} n_{j+1}^{\lvert 0\rangle}$	$n_{j-1}^{\lvert 1\rangle} n_{j+1}^{\lvert 1\rangle}$

$$\tag{3.8}$$

Each term can either be included or omitted in $\hat{P}_j$, leading to $2^4 = 16$ possible combinations. To increase this number to 256, which is the number of possible rules in the Wolfram code, more generalizations have to be made.

Each of the up to 4 different behaviors present in an NRT-decomposition requires a different operator $\hat{S}_j$. Each of those $\hat{S}_j$ in turn requires its own $\hat{P}_j$ controlling the set of neighborhoods to act on, leading to a modified version of Equation (3.7):

$$\hat{H}_j^{\text{generalized}} = \hat{S}_j^{\text{no change}} \hat{P}_j^{\text{no change}} + \hat{S}_j^{\text{bit flip}} \hat{P}_j^{\text{bit flip}} + \hat{S}_j^{\text{set to 0}} \hat{P}_j^{\text{set to 0}} + \hat{S}_j^{\text{set to 1}} \hat{P}_j^{\text{set to 1}} \tag{3.9}$$

Each term from Equation (3.8) is included in exactly one of the $\hat{P}_j$ from Equation (3.9), because each behavior is executed in exactly one neighborhood. For each term, one $\hat{P}_j$ is chosen, leading to $4^4 = 256$ possible values for $\hat{H}_j^{\text{generalized}}$ and covering every rule of the Wolfram Code.

The non-reversible nature of peripheral CAs hints that the time evolution of their quantum counterparts is non-unitary. As already mentioned, this marks a deviation from the generally accepted definition of QCAs. While closed systems undergoing a non-unitary time evolution are not physical, such systems can be understood as part of a larger system that in turn undergoes a unitary time evolution. The non-unitarity of the subsystem is then a consequence of only viewing a partial trace of the complete system [NC10]. This also means that a state might no longer be normalized after undergoing such a time evolution, so it has to be normalized before making any measurements. However, without constraining the time evolution to be unitary, $\hat{H}_j$ can be chosen to be non-hermitian, which will be necessary to find operators satisfying peripheral NRT-behaviors (cf. Section 3.4).

Foregoing arbitrary rules for now and focusing only the set of 16 possible rules given by Equation (3.7), it is already possible to create QCAs for an important class of Wolfram codes: reversible rules.

3.3 Reversible Rules

A rule is called reversible if its NRT-decomposition only consists of reversible NRTs (cf. Section 2.2.2). More specifically, every rule with a NRT-decomposition that only includes the "bit flip" and "no change" behaviors is reversible since those are the only reversible NRT-behaviors (cf. Equation (2.2)). An example of a reversible rule is 150, where this pattern can be observed by either checking its NRT-decomposition, shown in Figure 2.3b, or more intuitively by describing its behavior in words:

*A cell is **flipped if** exactly one of its neighbors is alive*

Rule		51	54	57	60	99	102	105	108	147	150	153	156	195	198	201	204
$\hat{P}_j$	$n^{\|1\rangle}_{j-1} n^{\|1\rangle}_{j+1}$	x	x	x	x	x	x	x	x								
	$n^{\|1\rangle}_{j-1} n^{\|0\rangle}_{j+1}$	x	x	x	x					x	x	x	x				
	$n^{\|0\rangle}_{j-1} n^{\|1\rangle}_{j+1}$	x	x			x	x			x	x			x	x		
	$n^{\|0\rangle}_{j-1} n^{\|0\rangle}_{j+1}$	x		x		x		x		x		x		x		x	

Figure 3.2 A bijective mapping between all reversible elementary CA rules and all the set of all possible $\hat{P}_j$. For a given rule, the table shows which of the 4 possible terms from Equation (3.8) are included in the corresponding $\hat{P}_j$, marked with x if included. $\hat{P}_j$ is constructed as a sum of all included terms.

Starting with Rule 150, the goal is to find operators $\hat{S}_j$ and $\hat{P}_j$ to use in Equation (3.7), such that $\hat{H}_j$ governs this desired time evolution in a quantum system.

The bit flip operator on a Qubit is given by the Pauli-x gate:

$$\sigma^x |0\rangle = |1\rangle \qquad \sigma^x |1\rangle = |0\rangle \qquad (3.10)$$

Performing a time evolution governed by σ^x results in a rotation operator on the Bloch sphere, continuously flipping $|0\rangle$ and $|1\rangle$[NC10]. When setting $\hat{S}_j = \sigma^x$, $\hat{P}_j$ can be chosen to only include terms corresponding to configurations where a bit flip should occur. For rule 150, $\hat{P}_j$ includes all terms where exactly one neighbor is alive:

$$\hat{P}_j = \left(n^{|0\rangle}_{j-1} n^{|1\rangle}_{j+1} + n^{|1\rangle}_{j-1} n^{|0\rangle}_{j+1} \right) \qquad (3.11)$$

Finally, by following the example from [Ney+22] and setting $t = \frac{\pi}{2}$, the dynamic under $\hat{U}_j = e^{-it\sigma^x \left(n^{|0\rangle}_{j-1} n^{|1\rangle}_{j+1} + n^{|1\rangle}_{j-1} n^{|0\rangle}_{j+1} \right)}$ of all possible cell triplets $|\psi\rangle_j$ at index j according to Equation (3.5) exactly follows a classical bit flip:

$|\psi\rangle_j$	$|1\rangle \otimes |n\rangle \otimes |1\rangle$	$|1\rangle \otimes |n\rangle \otimes |0\rangle$	$|0\rangle \otimes |n\rangle \otimes |1\rangle$	$|0\rangle \otimes |n\rangle \otimes |0\rangle$
$\downarrow$	$\downarrow$	$\downarrow$	$\downarrow$	$\downarrow$
$\hat{U}_j |\psi\rangle_j$	$|1\rangle \otimes |n\rangle \otimes |1\rangle$	$|1\rangle \otimes e^{-it\sigma^x} |n\rangle \otimes |0\rangle$	$|0\rangle \otimes e^{-it\sigma^x} |n\rangle \otimes |1\rangle$	$|0\rangle \otimes |n\rangle \otimes |0\rangle$
$t = \frac{\pi}{2}$	$|1\rangle \otimes |n\rangle \otimes |1\rangle$	$|1\rangle \otimes |n \oplus 1\rangle \otimes |0\rangle$	$|0\rangle \otimes |n \oplus 1\rangle \otimes |1\rangle$	$|0\rangle \otimes |n\rangle \otimes |0\rangle$

(3.12)

, where $|n\rangle \in \{|0\rangle, |1\rangle\}$ and $\oplus$ is addition modulo 2. Thus, unless otherwise specified, the time step size in the quantum case will be $t = \frac{\pi}{2}$ for all QCAs shown in this thesis.

The described method works for any reversible elementary rule. More generally, there exists a bijective mapping between the set of all possible $\hat{P}_j$ and the set of all reversible elementary CAs, shown in Figure 3.2. By fixing $\hat{S}_j = \sigma^x_j$ it is therefore possible to create a QCA for every possible reversible Wolfram rule.

3.4 Peripheral Rules

The choice of fixing $\hat{S}_j = \sigma^x_j$ to model reversible QCAs is intuitive in the sense that the Pauli-x gate describes a Qubit bit flip, an analogue to the bit flips occurring in classical reversible CAs. In contrast, for modeling non-reversible QCAs the choice of $\hat{S}_j$ is not as obvious. Focusing on purely peripheral rules for now, the relevant NRTs behaviors are "set to 0" and "set to 1" (cf. Equation (2.2)). The goal is then to find a set of two operators $\left\{ \hat{S}^{\text{set to }0}_j, \hat{S}^{\text{set to }1}_j \right\}$ such that their respective time evolution operators given by Equation (3.5) will lead to those behaviors. In contrast to the reversible case, there is more than one possible set of operators realizing this.

Given an arbitrary normalized initial state $|\psi\rangle = (\alpha\,|0\rangle + \beta\,|1\rangle)$, with $\alpha, \beta \in \mathbb{C}$ and $|\alpha|^2 + |\beta|^2 = 1$, the effect of a time evolution on $|\psi\rangle$ governed by those operators according to Equation (3.5) can be calculated. For ease of notation, in the following calculations $\left\{ \hat{S}_j^{\text{set to 0}}, \hat{S}_j^{\text{set to 1}} \right\}$ will be replaced with $\{\hat{S}_{|0\rangle}, \hat{S}_{|1\rangle}\}$, dropping the j and shortening the description.

3.4.1 Elementary Matrix Operator Set

One possible set of operators are the non-diagonal elementary matrices

$$\hat{S}_{|0\rangle} = |0\rangle\langle 1| \qquad \hat{S}_{|1\rangle} = |1\rangle\langle 0| \tag{3.13}$$

According to Equation (3.5), the time evolution operators governed by them are

$$\hat{U}_{|0\rangle} = e^{(-it\hat{S}_{|0\rangle})} = e^{(-it|0\rangle\langle 1|)} = \sum_{n=0}^{\infty} \frac{(-it\,|0\rangle\langle 1|)^n}{n!} = I - it\,|0\rangle\langle 1| \tag{3.14}$$

and

$$\hat{U}_{|1\rangle} = e^{(-it\hat{S}_{|1\rangle})} = e^{(-it|1\rangle\langle 0|)} = \sum_{n=0}^{\infty} \frac{(-it\,|1\rangle\langle 0|)^n}{n!} = I - it\,|1\rangle\langle 0| \tag{3.15}$$

where it was used that

$$\forall n \in \mathbb{N} \left(n > 1 \longrightarrow (|0\rangle\langle 1|)^n = (|1\rangle\langle 0|)^n = 0 \right). \tag{3.16}$$

The time evolution under those operators with subsequent normalization is given by

$$|\psi\rangle_{|0\rangle\langle 1|}(t) = e^{-it|0\rangle\langle 1|}\,|\psi\rangle = (I - it\,|0\rangle\langle 1|)\,|\psi\rangle = (\alpha - it\beta)\,|0\rangle + \beta\,|1\rangle \xrightarrow{normalize} \frac{(\alpha - it\beta)\,|0\rangle + \beta\,|1\rangle}{\sqrt{|\alpha - it\beta|^2 + |\beta|^2}} \tag{3.17}$$

and

$$|\psi\rangle_{|1\rangle\langle 0|}(t) = e^{-it|1\rangle\langle 0|}\,|\psi\rangle = (I - it\,|1\rangle\langle 0|)\,|\psi\rangle = \alpha\,|0\rangle + (\beta - it\alpha)\,|1\rangle \xrightarrow{normalize} \frac{\alpha\,|0\rangle + (\beta - it\alpha)\,|1\rangle}{\sqrt{|\alpha|^2 + |\beta - it\alpha|^2}} \tag{3.18}$$

The probabilities for $|\psi\rangle$ to be in state $|0\rangle$ or $|1\rangle$ at time t during these time evolutions can then be calculated:

$$Pr\left[|\psi\rangle_{|0\rangle\langle 1|}(t) = |0\rangle \right] = \left| \langle 0| \left(\frac{(\alpha - it\beta)\,|0\rangle + \beta\,|1\rangle}{\sqrt{|\alpha - it\beta|^2 + |\beta|^2}} \right) \right|^2 = \left| \frac{\alpha - it\beta}{\sqrt{|\alpha - it\beta|^2 + |\beta|^2}} \right|^2 = \frac{|\alpha - it\beta|^2}{|\alpha - it\beta|^2 + |\beta|^2} \tag{3.19}$$

$$Pr\left[|\psi\rangle_{|0\rangle\langle 1|}(t) = |1\rangle \right] = \left| \langle 1| \left(\frac{(\alpha - it\beta)\,|0\rangle + \beta\,|1\rangle}{\sqrt{|\alpha - it\beta|^2 + |\beta|^2}} \right) \right|^2 = \left| \frac{\beta}{\sqrt{|\alpha - it\beta|^2 + |\beta|^2}} \right|^2 = \frac{|\beta|^2}{|\alpha - it\beta|^2 + |\beta|^2} \tag{3.20}$$

$$Pr\left[|\psi\rangle_{|1\rangle\langle 0|}(t) = |0\rangle \right] = \left| \langle 0| \left(\frac{\alpha\,|0\rangle + (\beta - it\alpha)\,|1\rangle}{\sqrt{|\alpha|^2 + |\beta - it\alpha|^2}} \right) \right|^2 = \left| \frac{\alpha}{\sqrt{|\alpha|^2 + |\beta - it\alpha|^2}} \right|^2 = \frac{|\alpha|^2}{|\alpha|^2 + |\beta - it\alpha|^2} \tag{3.21}$$

$$Pr\left[|\psi\rangle_{|1\rangle\langle 0|}(t) = |1\rangle \right] = \left| \langle 1| \left(\frac{\alpha\,|0\rangle + (\beta - it\alpha)\,|1\rangle}{\sqrt{|\alpha|^2 + |\beta - it\alpha|^2}} \right) \right|^2 = \left| \frac{\beta - it\alpha}{\sqrt{|\alpha|^2 + |\beta - it\alpha|^2}} \right|^2 = \frac{|\beta - it\alpha|^2}{|\alpha|^2 + |\beta - it\alpha|^2} \tag{3.22}$$

Thus, convergence is achieved regardless of the initial state:

$$\lim_{t \to \infty} Pr\left[|\psi\rangle_{|0\rangle\langle 1|}(t) = |0\rangle \right] = \lim_{t \to \infty} \frac{|\alpha - it\beta|^2}{|\alpha - it\beta|^2 + |\beta|^2} = 1 \tag{3.23}$$

$$\lim_{t\to\infty} Pr\left[|\psi\rangle_{|0\rangle\langle 1|}(t) = |1\rangle\right] = \lim_{t\to\infty} \frac{|\beta|^2}{|\alpha - it\beta|^2 + |\beta|^2} = 0 \tag{3.24}$$

$$\lim_{t\to\infty} Pr\left[|\psi\rangle_{|1\rangle\langle 0|}(t) = |0\rangle\right] = \lim_{t\to\infty} \frac{|\alpha|^2}{|\alpha|^2 + |\beta - it\alpha|^2} = 0 \tag{3.25}$$

$$\lim_{t\to\infty} Pr\left[|\psi\rangle_{|1\rangle\langle 0|}(t) = |1\rangle\right] = \lim_{t\to\infty} \frac{|\beta - it\alpha|^2}{|\alpha|^2 + |\beta - it\alpha|^2} = 1 \tag{3.26}$$

This convergence makes intuitive sense, as the effect of Equations (3.14) and (3.15) on $|\psi\rangle$ can be described as keeping one basis state constant while growing the other linearly with t. However, this also hints to the problem of scaling some basis states much more than others. When inserting $\hat{S}_{|0\rangle}$ and $\hat{S}_{|1\rangle}$ into Equation (3.9), they will govern the time evolution alongside the operators for the reversible case $\hat{S}_j^{\text{no change}}$ and $\hat{S}_j^{\text{bit flip}}$. Both of these reversible operators are hermitian, which makes the time evolution governed by them unitary, therefore norm preserving and not scaling any basis vector. This means that a time evolution governed by a rule with both reversible and peripheral terms will scale the effect of reversible operations differently than peripheral ones. The terms making up the superposition of the resulting state will therefore be weighted differently, making the effect of one behavior more prevalent than the other. This does not align with the classical behavior where there is no distinction between the weight of different behaviors.

By inspecting the operator's singular values, their worst-case scaling effect can be observed. $\hat{U}_{|0\rangle}$ and $\hat{U}_{|1\rangle}$ have the same singular values:

$$\hat{U}_{|0\rangle}^\dagger \hat{U}_{|0\rangle} = \left(\hat{U}_{|1\rangle}\hat{U}_{|1\rangle}^\dagger\right)^\mathsf{T} \tag{3.27}$$

Thus, it suffices to calculate the singular values $s_{1,2}(t)$ for a generic $\hat{U}_{|k\rangle} \in \{\hat{U}_{|0\rangle}, \hat{U}_{|0\rangle}\}$:

$$\det\left(\hat{U}_{|k\rangle}^\dagger \hat{U}_{|k\rangle} - \lambda I\right) = \lambda^2 - \lambda\left(t^2 + 2\right) + 1 \overset{!}{=} 0 \tag{3.28}$$

$$\lambda_{1,2}(t) = \frac{t^2 + 2 \pm \sqrt{\left(t^2+2\right)^2 - 4}}{2} = \frac{t^2 + 2 \pm t\sqrt{t^2+4}}{2} = \frac{\left(t \pm \sqrt{t^2+4}\right)^2}{4} \tag{3.29}$$

$$s_{1,2}(t) = \sqrt{\lambda_{1,2}(t)} = \pm\frac{t \pm \sqrt{t^2+4}}{2} \tag{3.30}$$

Discarding invalid singular values leaves

$$s_1(t) = \frac{\sqrt{t^2+4} + t}{2} \qquad s_2(t) = \frac{\sqrt{t^2+4} - t}{2} \tag{3.31}$$

Viewing the limit of $t \to \infty$

$$\lim_{t\to\infty} s_1(t) = \lim_{t\to\infty} \frac{\sqrt{t^2+4} + t}{2} = \infty \qquad \lim_{t\to\infty} s_2(t) = \lim_{t\to\infty} \frac{\sqrt{t^2+4} - t}{2} = 0 \tag{3.32}$$

aligns with expectations. One singular value reaches 0 due to the projection on $|0\rangle$ or $|1\rangle$, respectively. However, the other value is scaled to infinity.

3.4.2 Projection Operator Set

Another approach for finding a set of operators $\left\{\hat{H}'_{|0\rangle}, \hat{H}'_{|1\rangle}\right\}$ is to work backwards from a given $\hat{U}'$. An intuitive choice for a set of operators $\left\{\hat{U}'_{|0\rangle}, \hat{U}'_{|1\rangle}\right\}$ realizing the behaviors "set to $\{|0\rangle, |1\rangle\}$", are the projectors on $\{|0\rangle, |1\rangle\}$:

$$\hat{U}'_{|0\rangle} := |0\rangle\langle 0| + |0\rangle\langle 1| \qquad \hat{U}'_{|1\rangle} := |1\rangle\langle 0| + |1\rangle\langle 1| \tag{3.33}$$

Rearranging Equation (3.5) and solving for $\hat{H}_j$

$$\hat{H}_j = \frac{\ln\left(\hat{U}_j\right)}{-it} \tag{3.34}$$

does not work for $\hat{U}_{|0\rangle}$ and $\hat{U}_{|1\rangle}$, as both operators have undefined logarithms. If one is willing to do without an exact solution, however, there are operators that still show the desired behavior in the limit of $t \to \infty$:

$$\hat{H}_{|0\rangle} := i\,|0\rangle\,\langle 1| - i\,|1\rangle\,\langle 1| \qquad \hat{H}_{|1\rangle} := i\,|1\rangle\,\langle 0| - i\,|0\rangle\,\langle 0| \tag{3.35}$$

For $\hat{H}_{|k\rangle} \in \left\{\hat{H}_{|0\rangle}, \hat{H}_{|1\rangle}\right\}$, and with

$$\forall n \in \mathbb{N}\left(n > 0 \longrightarrow \left(\hat{H}_{|k\rangle}\right)^n = (-i)^n i\,\hat{H}_{|k\rangle}\right) \tag{3.36}$$

the time evolution operators governed by $\hat{H}_{|0\rangle}$ and $\hat{H}_{|1\rangle}$ according to Equation (3.5) are given by:

$$e^{\left(-it\hat{H}_{|k\rangle}\right)} = \sum_{n=0}^{\infty} \frac{\left(-it\hat{H}_{|k\rangle}\right)^n}{n!} = I + \sum_{n=1}^{\infty} \frac{(-it)^n(-i)^n i\,\hat{H}_{|k\rangle}}{n!} = I + \left(\sum_{n=1}^{\infty} \frac{(-t)^n}{n!}\right) i\,\hat{H}_{|k\rangle} = I + \left(e^{-t} - 1\right) i\,\hat{H}_{|k\rangle} \tag{3.37}$$

Convergence for $t \to \infty$ is then immediately apparent:

$$\lim_{t \to \infty} e^{\left(-it\hat{H}_{|0\rangle}\right)} = \lim_{t \to \infty} \left(e^{-t} - 1\right) i\,\hat{H}_{|0\rangle} = |0\rangle\,\langle 0| + |0\rangle\,\langle 1| \tag{3.38}$$

$$\lim_{t \to \infty} e^{\left(-it\hat{H}_{|1\rangle}\right)} = \lim_{t \to \infty} \left(e^{-t} - 1\right) i\,\hat{H}_{|1\rangle} = |1\rangle\,\langle 0| + |1\rangle\,\langle 1| \tag{3.39}$$

The time evolution of $|\psi\rangle$ under those operators with subsequent normalization is given by:

$$|\psi\rangle_{|0\rangle}(t) = \frac{\left(\alpha - \beta e^{-t} + \beta\right)|0\rangle + \beta e^{-t}\,|1\rangle}{\sqrt{|\alpha - \beta e^{-t} + \beta|^2 + |\beta e^{-t}|^2}} \tag{3.40}$$

and

$$|\psi\rangle_{|1\rangle}(t) = \frac{\alpha e^{-t}\,|0\rangle + \left(\beta - \alpha e^{-t} + \alpha\right)|1\rangle}{\sqrt{|\alpha e^{-t}|^2 + |\beta - \alpha e^{-t} + \alpha|^2}} \tag{3.41}$$

The probabilities for $|\psi\rangle$ to be in state $|0\rangle$ or $|1\rangle$ at time t during these time evolutions is given by:

$$Pr\left[|\psi\rangle_{|0\rangle}(t) = |0\rangle\right] = \frac{|\alpha - \beta e^{-t} + \beta|^2}{|\alpha - \beta e^{-t} + \beta|^2 + |\beta e^{-t}|^2} \tag{3.42}$$

$$Pr\left[|\psi\rangle_{|0\rangle}(t) = |1\rangle\right] = \frac{|\beta e^{-t}|^2}{|\alpha - \beta e^{-t} + \beta|^2 + |\beta e^{-t}|^2} \tag{3.43}$$

$$Pr\left[|\psi\rangle_{|1\rangle}(t) = |0\rangle\right] = \frac{|\alpha e^{-t}|^2}{|\alpha e^{-t}|^2 + |\beta - \alpha e^{-t} + \alpha|^2} \tag{3.44}$$

$$Pr\left[|\psi\rangle_{|1\rangle}(t) = |1\rangle\right] = \frac{|\beta - \alpha e^{-t} + \alpha|^2}{|\alpha e^{-t}|^2 + |\beta - \alpha e^{-t} + \alpha|^2} \tag{3.45}$$

Complete versions of Equations (3.40) to (3.45) are shown in Equations (A.1) to (A.6) in Appendix A.1.

Thus, convergence is achieved regardless of the initial state:

$$\lim_{t \to \infty} Pr\left[|\psi\rangle_0(t) = |0\rangle\right] = \lim_{t \to \infty} \frac{|\alpha - \beta e^{-t} + \beta|^2}{|\alpha - \beta e^{-t} + \beta|^2 + |\beta e^{-t}|^2} = 1 \tag{3.46}$$

13

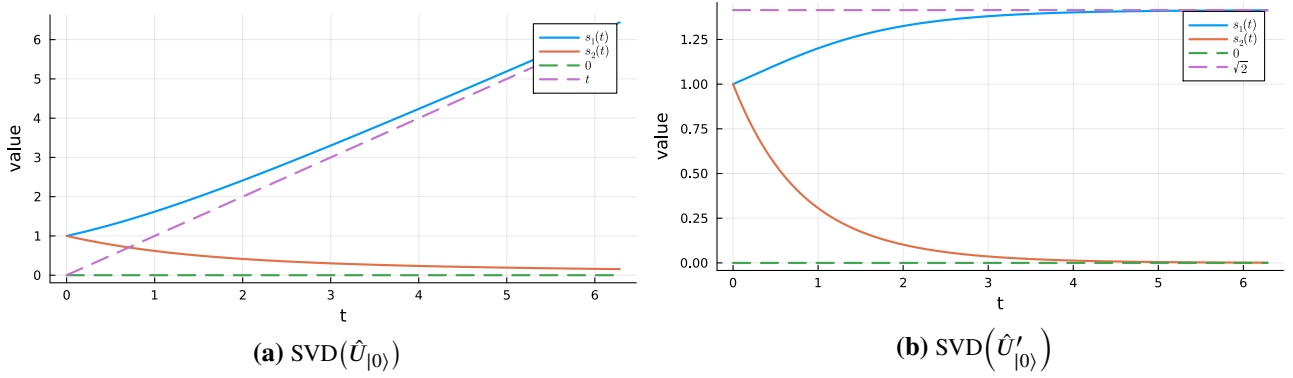**(a)** SVD$\left(\hat{U}_{|0\rangle}\right)$ **(b)** SVD$\left(\hat{U}'_{|0\rangle}\right)$

Figure 3.3 Singular values of $\hat{U}_{|0\rangle}$ and $\hat{U}'_{|0\rangle}$, according to Equation (A.9) in Appendix A.2

$$\lim_{t\to\infty} Pr\left[|\psi\rangle_0(t) = |1\rangle\right] = \lim_{t\to\infty} \frac{\left|\beta e^{-t}\right|^2}{\left|\alpha - \beta e^{-t} + \beta\right|^2 + \left|\beta e^{-t}\right|^2} = 0 \tag{3.47}$$

$$\lim_{t\to\infty} Pr\left[|\psi\rangle_1(t) = |0\rangle\right] = \lim_{t\to\infty} \frac{\left|\alpha e^{-t}\right|^2}{\left|\alpha e^{-t}\right|^2 + \left|\beta - \alpha e^{-t} + \alpha\right|^2} = 0 \tag{3.48}$$

$$\lim_{t\to\infty} Pr\left[|\psi\rangle_1(t) = |1\rangle\right] = \lim_{t\to\infty} \frac{\left|\beta - \alpha e^{-t} + \alpha\right|^2}{\left|\alpha e^{-t}\right|^2 + \left|\beta - \alpha e^{-t} + \alpha\right|^2} = 1 \tag{3.49}$$

Like for the case of $\hat{U}_{|0\rangle}$ and $\hat{U}_{|1\rangle}$, the time evolution governed by operator set 2 keeps one basis state constant and grows the other one, leading to a convergence. Unfortunately, in contrast to the first set, the closed formula for the singular values of $\hat{U}'_{|0\rangle}$ and $\hat{U}'_{|1\rangle}$ is long and does not provide any additional insight (cf Equations (A.7) to (A.10) in Appendix A.2). However, $\hat{U}'_{|0\rangle}(t)$ and $\hat{U}'_{|1\rangle}(t)$ converge to $|0\rangle\langle 0| + |0\rangle\langle 1|$ and $|1\rangle\langle 0| + |1\rangle\langle 1|$ for $t \to \infty$, according to Equations (3.38) and (3.39). Thus, their singular values in the limit of $t \to \infty$ can be calculated.

Singular values are invariant under transposition, so it suffices to calculate them for $\hat{U}_{|0\rangle}$.

$$\sqrt{\hat{U}'^{\dagger}_{|0\rangle}\hat{U}'_{|0\rangle}} = \sqrt{2}\,|0\rangle\langle 0| \implies s_{1,2} = \left\{0, \sqrt{2}\right\} \tag{3.50}$$

The first singular value converges to 0 because of the projection onto the respective basis states, just like for operator set 1. The other value converges to $\sqrt{2}$, a constant value close to 1, producing a less significant scaling effect than the one observed for the elementary matrix operator set (cf. Section 3.4.1).

3.4.3 Comparison

Both operator sets are a possible choice to use in Equation (3.9), both with their strengths and drawbacks. Figure 3.4 shows time evolutions of some state $|\psi\rangle$, given as probabilities of $|\psi\rangle$ being in state $|0\rangle$ or $|1\rangle$, respectively. The left side shows plots of Equations (3.19) and (3.20) governed by $\hat{H}_{|0\rangle}$, the right side shows plots of Equations (3.42) and (3.43) governed by $\hat{H}'_{|0\rangle}$. Evolutions governed by $\hat{H}_{|1\rangle}$ and $\hat{H}'_{|1\rangle}$ are not shown, as these would look equivalent to switching the line colors in Figure 3.4.

Convergence is quick in almost all cases. Set 2 (right side) converges faster than set 1 (left) in general, caused by the exponential term in Equations (3.42) and (3.43). Special cases include Figure 3.4d, where α and β are chosen opposite, such that the fractions in Equations (3.42) and (3.43) reduce to $\frac{1}{2}$. Another special case is shown in Figure 3.4e, where α and β are chosen in a way that the numerator in Equation (3.19) initially decreases before convergence starts like in the other cases.

Figure 3.3 shows plots of the singular values of $\hat{U}_{|0\rangle}$ and $\hat{U}'_{|0\rangle}$ as a function of t, and confirms that the scaling behavior of $\hat{U}_{|0\rangle}$ is worse than for $\hat{U}'_{|0\rangle}$. Thus, I chose to use operator set 2 for $\hat{S}_j^{\text{set to } 0}$ and $\hat{S}_j^{\text{set to } 0}$ in Equation (3.9) for all further calculations and plots for this thesis.

(a) $|\psi\rangle_0 = |0\rangle$

(b) $|\psi\rangle_0 = |1\rangle$

(c) $|\psi\rangle_0 = \frac{1}{\sqrt{2}}(|0\rangle + |1\rangle)$

(d) $|\psi\rangle_0 = \frac{1}{\sqrt{2}}(|0\rangle - |1\rangle)$

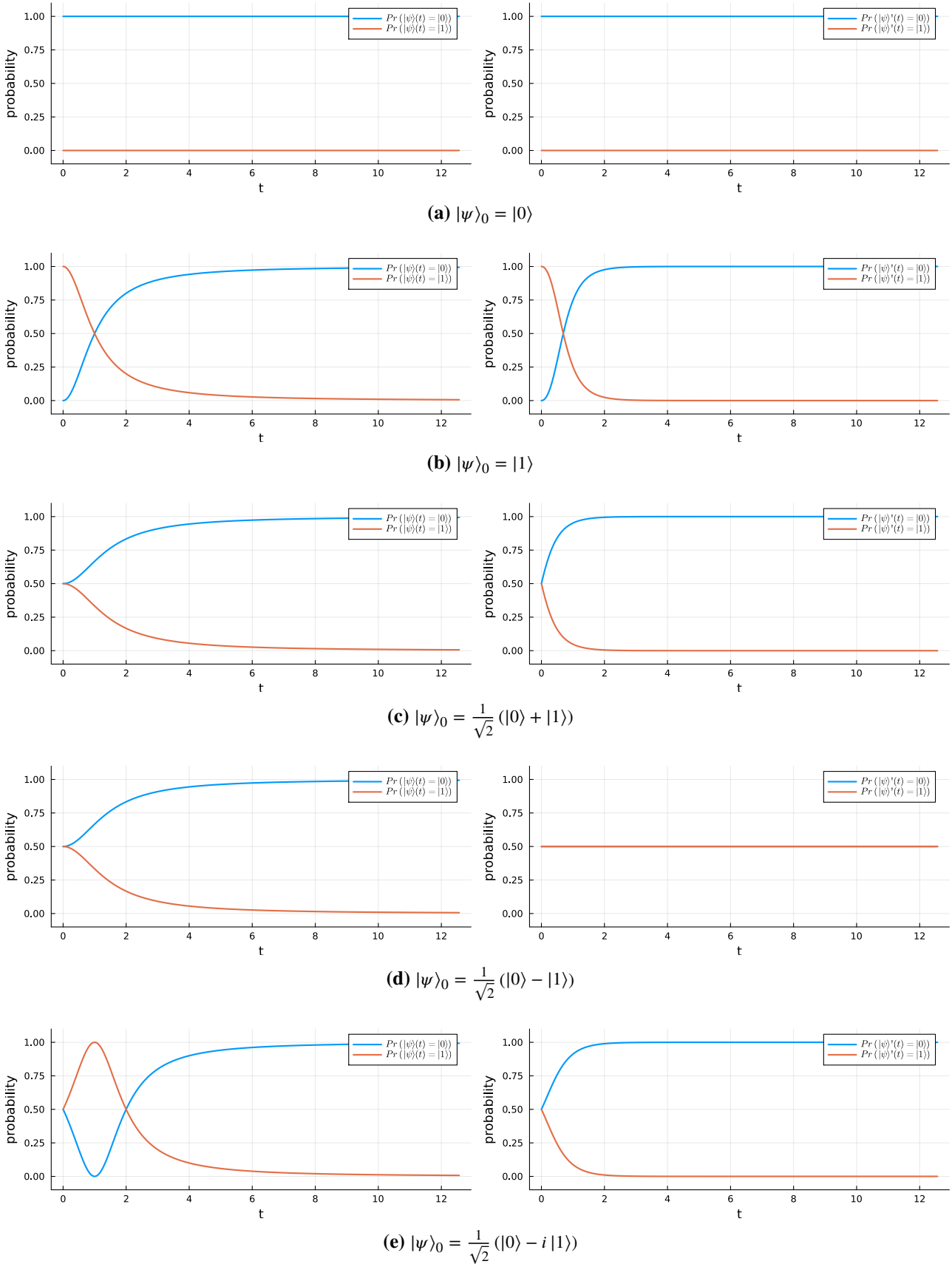**(e)** $|\psi\rangle_0 = \frac{1}{\sqrt{2}}(|0\rangle - i|1\rangle)$

Figure 3.4 Probability of $|\psi\rangle(t)$ to be in state $|0\rangle$ or $|1\rangle$, where $|\psi\rangle_0$ labels the initial state. The left side shows a time evolution governed by $\hat{S}_{|0\rangle}$ introduced in Section 3.4.1, the right side governed by $\hat{S}'_{|0\rangle}$, introduced in Section 3.4.2.

3.5 Arbitrary Rules

With working operators for all necessary $\hat{S}_j$ in Equation (3.9), QCAs for arbitrary Wolfram rules can be created. Given some rule, the corresponding QCA can be created by distributing the terms from Equation (3.8) to their corresponding operator $\hat{P}_j$, as dictated by the rule's NRT-decomposition. For rule 110 and 150 with their NRT-decompositions shown in Figure 2.3, this results in

$$
\begin{aligned}
\hat{H}_j^{\text{R110}} &= 0 \left(n_{j-1}^{|0\rangle} n_{j+1}^{|0\rangle} + n_{j-1}^{|1\rangle} n_{j+1}^{|0\rangle} \right) + \sigma_j^x \left(n_{j-1}^{|1\rangle} n_{j+1}^{|1\rangle} \right) + |0\rangle_j \langle 1|_j\, 0 + |1\rangle_j \langle 0|_j \left(n_{j-1}^{|0\rangle} n_{j+1}^{|1\rangle} \right) \\
&= \sigma_j^x \left(n_{j-1}^{|1\rangle} n_{j+1}^{|1\rangle} \right) + |1\rangle_j \langle 0|_j \left(n_{j-1}^{|0\rangle} n_{j+1}^{|1\rangle} \right)
\end{aligned}
\tag{3.51}
$$

and

$$
\begin{aligned}
\hat{H}_j^{\text{R150}} &= 0 \left(n_{j-1}^{|0\rangle} n_{j+1}^{|0\rangle} + n_{j-1}^{|1\rangle} n_{j+1}^{|1\rangle} \right) + \sigma_j^x \left(n_{j-1}^{|0\rangle} n_{j+1}^{|1\rangle} + n_{j-1}^{|1\rangle} n_{j+1}^{|0\rangle} \right) + |0\rangle_j \langle 1|_j\, 0 + |1\rangle_j \langle 0|_j\, 0 \\
&= \sigma_j^x \left(n_{j-1}^{|0\rangle} n_{j+1}^{|1\rangle} + n_{j-1}^{|1\rangle} n_{j+1}^{|0\rangle} \right)
\end{aligned}
\tag{3.52}
$$

Notably, $\hat{H}_j^{\text{R150}}$ indeed matches $\hat{H}_j$ from Section 3.3.

4 Results, Comparisons and

The rather abstract analysis in the previous chapters was necessary to justify the choices made in creating this thesis' version of elementary QCAs, and as such, a properly motivated analogue to classical elementary CAs. While there will follow some more analysis in the latter part of this chapter (Section 4.2), for now, the results from the previous chapters allow visually inspecting the quantum time evolution for some rules, and comparing them to their classical counterparts.

The number of cells shown will differ for some of these plots, depending on which algorithm was used to calculate them. For plots of up to 14 cells, an exact calculation was used, solving Equation (3.5) exactly. This quickly becomes infeasible for large cell numbers, so depending on the growth of the state's bond dimensions the TDVP algorithm in its typical 1-site, or 2-site variant [Hae+11; Hae16], or an adaption of those [Dec23] was used. Unless otherwise specified, plots of the time evolution of the quantum versions use a time step size of $\frac{\pi}{2}$. Boundary conditions are closed with boundary cells in state $|0\rangle$. "Classical" labels a time evolution based on the rules of classical elementary CAs where each cell is either in state 0 or 1 at any given time step. "Expectation Value" labels the probability of a cell to collapse into state $|1\rangle$ if measured, given by Equation (3.4). All plots were made using [Dec24], making use of [FWS22a; FWS22b] for all calculations related to tensors networks.

4.1 Similarities between classical and quantum evolutions

4.1.1 Frozen states in rule 108

$$\hat{H}_j^{\mathrm{R}108} = \sigma_j^x \left(n_{j-1}^{|1\rangle} n_{j+1}^{|1\rangle} \right) \tag{4.1}$$

While the plot of an elementary QCA will generally differ from its classical counterpart, there are some rules where the plot of their respective time evolutions look identical for a subset of initial states. In most of those cases, the classical behavior is not complex to begin with, one of the most trivial examples can be found in rule 108:

A cell is flipped if both of its neighbors are alive

Some of the eigenstates of $\hat{H}_j^{\mathrm{R}108}$ are also product states in the $\{|0\rangle, |1\rangle\}$ basis, so called frozen states [Sal+20]. In particular, any product state where no cell has two neighbors in state $|1\rangle$ is annihilated by $\hat{H}_j^{\mathrm{R}108}$. One example
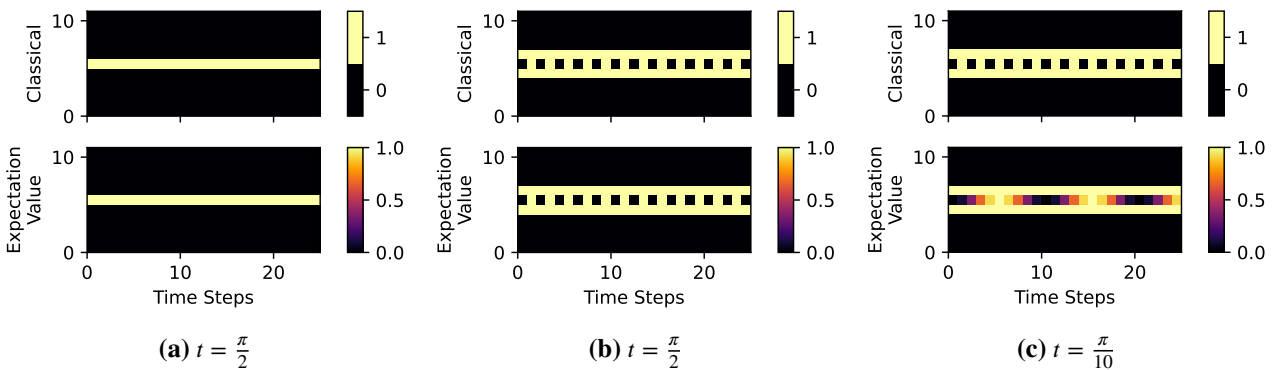

Figure 4.1 Comparison of classical and quantum time evolutions of rule 108 for different initial states. Classical step size is always constant, quantum step size is labeled t.
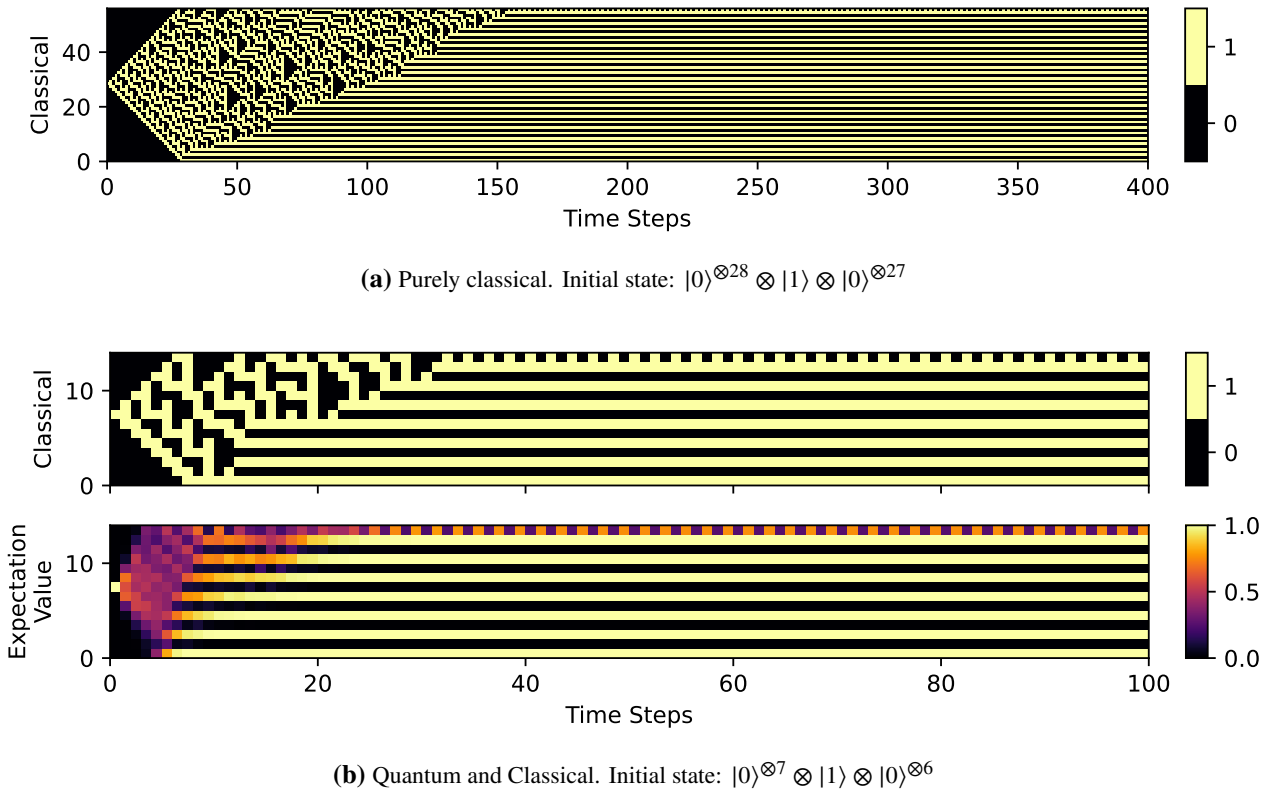
17

(a) Purely classical. Initial state: $|0\rangle^{\otimes 28} \otimes |1\rangle \otimes |0\rangle^{\otimes 27}$

(b) Quantum and Classical. Initial state: $|0\rangle^{\otimes 7} \otimes |1\rangle \otimes |0\rangle^{\otimes 6}$

Figure 4.2 Comparison of the classical and quantum versions of the rule 30 elementary CA for different initial states

of the time evolution of a frozen state is plotted in Figure 4.1a, where the quantum and classical time evolutions are identical.

Figure 4.1b shows the evolution of an almost frozen state where only the center cell can change. The middle cell will get flipped continuously while the rest of the system stays constant. The classical and quantum behaviors again appear completely identical, however, the real dynamic of the quantum plot becomes visible in Figure 4.1c where the step size is chosen unequal to a multiple of $\frac{\pi}{2}$, the time needed to complete one flip in the time evolution governed by σ^x (Section 3.3). This again reinforces the choice for made for t in Section 3.3.

If periodic or open boundary conditions are used, every rule has an "opposite", in the sense that an opposite rule shows the same dynamic to the original rule if the meaning of $|0\rangle$ and $|1\rangle$ are flipped. The opposite rule of 108 is 201, which is also known as the PXP-model. While both rules share the same interesting properties, they are mostly studied from the viewpoint of the PXP-model, instead of $\hat{H}_j^{R108}$, which is why a more in-depth discussion of the rule's properties is deferred to Section 4.2.3, which discusses rule 201.

4.1.2 Convergence to a stable state in rule 30

$$\hat{H}_j^{R30} = \sigma_j^x \left(n_{j-1}^{|1\rangle} n_{j+1}^{|0\rangle} \right) + \hat{H}_{|0\rangle}' \left(n_{j-1}^{|1\rangle} n_{j+1}^{|1\rangle} \right) + \hat{H}_{|1\rangle}' \left(n_{j-1}^{|0\rangle} n_{j+1}^{|1\rangle} \right) \tag{4.2}$$

In [WW17], Stephen Wolfram called rule 30 his "all-time favorite discovery". The classical time evolution shown in Figure 4.2a indeed shows a surprising complexity. Complex patterns emerge while seeming to expand in space until the lower side of the expansion hits the lower boundary, which causes the cells to start collapsing into a fixed pattern after which only the top row remains active.

Figure 4.2b shows time evolutions for the classical and quantum case of rule 30. Unfortunately, in the quantum version cells tend to quickly build up a lot of entanglement right at the start of the time evolution, which makes even approximative algorithms unfeasible for large cell numbers. Therefore, the quantum plot shown in Figure 4.2b is limited to around 14 cells.
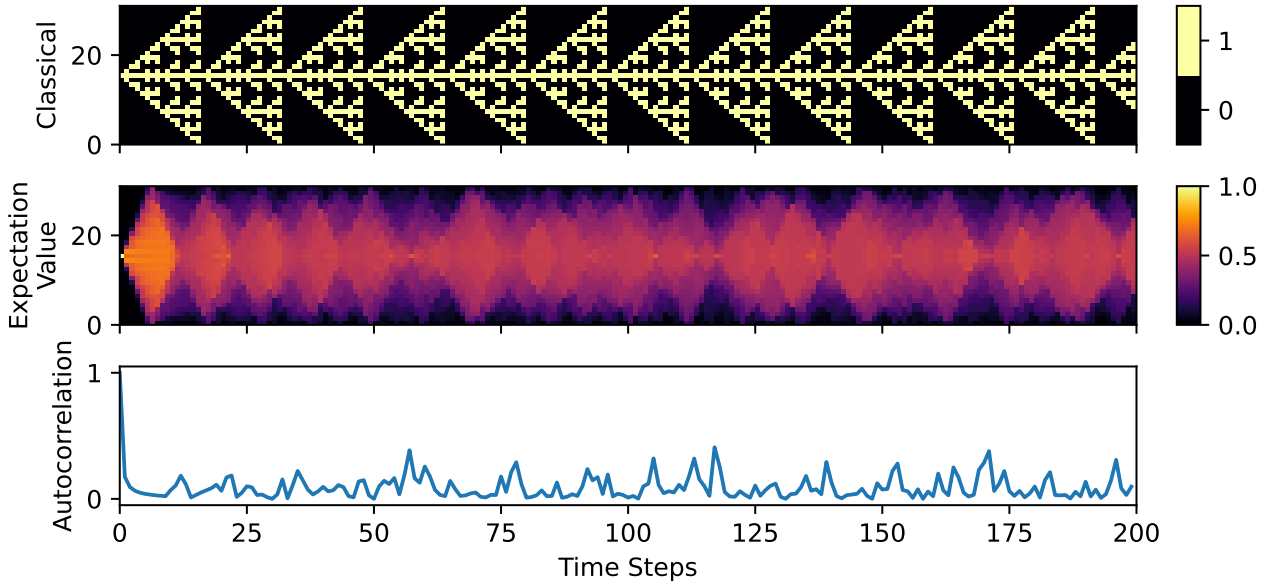
Figure 4.3 Comparison of the classical and quantum versions of the rule 150 elementary CA for the initial state $|\psi\rangle_0 = |0\rangle^{\otimes 15} \otimes |1\rangle \otimes |0\rangle^{\otimes 15}$. Autocorrelation is calculated as: $\left| \langle\psi|_0 \ |\psi\rangle_t \right|$.

Notably, the quantum evolution follows the classical one in collapsing to the same stable state and even shows a similar behavior in the topmost cell. This is surprising, as their time evolutions differ right at the start, but still converge to the same state over time. Section 3.4 discussed the role of the singular values of local operators on the unequal scaling of different terms in a state's superposition. Presumably, the exponential decay in one of the singular values of $\hat{U}_{|0\rangle}$ and $\hat{U}_{|1\rangle}$ (cf. Figure 3.3b) affects the time evolution of the complete system in a way that causes almost all cell configurations other than the fixed one seen in the plots to vanish over time. This pattern of vanishing complexity is common in plots for non-unitary elementary QCAs.

4.1.3 Periodic behavior in rule 150

$$\hat{H}_j^{\text{R150}} = \sigma_j^x \left(n_{j-1}^{|0\rangle} n_{j+1}^{|1\rangle} + n_{j-1}^{|1\rangle} n_{j+1}^{|0\rangle} \right) \tag{4.3}$$

For a subset of initial states, cells tend not to build up much entanglement with each other during time evolution of the rule 150 QCA. This makes it possible to simulate a large number of cells with high precision via approximative algorithms. In the case of Figure 4.3, the 1-site TDVP algorithm with a fixed bond dimension of 5 was used.

While the quantum time evolutions of rules 108 and 30 is very similar to their classical counterpart, this is not the case for all rules. When comparing the classical and quantum time evolutions of rule 150 in Figure 4.3, similarities are much less pronounced than for rules 108 and 30.

The classical version shows a periodic expansion and contraction, while the quantum version initially seems to mimic this periodically expanding behavior, before showing a more complicated, overlapping, and non-periodic dynamic. The system repeatedly approaches a configuration similar to its initial state but never completely returns to it, manifesting as fluctuations in the autocorrelation function. This phenomenon is called quantum revival, predicted by the quantum version of the Poincaré recurrence theorem, stating that the time evolution of a system with discrete energy eigenvalues will return arbitrarily close to its initial state, given enough time [BL57; Sch78; Per61; VPM15]. Generally, times between revivals in other quantum systems are very long, even for low similarity tolerances, which makes it surprising that the measured autocorrelation in Figure 4.3 shows visible peaks. The reason for this phenomenon is a breaking of ergodicity caused by Hilbert space fragmentation, which will be discussed in more detail in Section 4.2.3.

4.2 Analysis of purely quantum phenomena

4.2.1 Conflicting semi-stable states in Rule 23

$$\hat{H}_j^{\mathrm{R23}} = \sigma_j^x \left(n_{j-1}^{|1\rangle} n_{j+1}^{|0\rangle} + n_{j-1}^{|0\rangle} n_{j+1}^{|1\rangle} \right) + \hat{H}'_{|0\rangle} \left(n_{j-1}^{|1\rangle} n_{j+1}^{|1\rangle} \right) + \hat{H}'_{|1\rangle} \left(n_{j-1}^{|0\rangle} n_{j+1}^{|0\rangle} \right) \tag{4.4}$$

Rule 23 is an example of a system where the classical and quantum time evolutions have almost no similarities, which is why the plots shown here are missing the classical time evolution. Complete versions that include the classical evolutions are shown in Figure B.2 in **??**. However, the quantum version still has some interesting properties of its own.

Limiting number of cells to uneven numbers for now, after inspecting Equation (4.4) one might spot the Néel state $|10101\ldots\rangle$ as an eigenstate of $\hat{H}_j^{\mathrm{R23}}$. Similar to the case of rule 30, this is also the state the system converges towards, as all other configurations will get annihilated. An example of this is plotted in Figure 4.4a. Notably, the system approaches the state $|1010101010101\rangle$ instead of $|0101010101010\rangle$ because of the closed boundary conditions with boundary cells in state $|0\rangle$, causing the topmost and bottommost cells to flipped in the latter case.

In systems with an even number of cells on the other hand, this same boundary condition prevents the systems from converging to a stable state, as the outermost cells can no longer both be in state $|1\rangle$ while the system is also in a Néel state. This leads to a situation like the one plotted in Figure 4.4b, where stable states seem to grow from the bottom and top of the cell chain, separated by a boundary that moves up and down the cell chain. This manifests in a strongly fluctuating correlation with the initial state, which was chosen as one of the two possible Néel states.

Switching to periodic boundary conditions also seems to switch the roles of even and uneven numbers of cells in terms of convergence behavior. For an uneven number of cells, the Néel state is now no longer an eigenstate of $\hat{H}_j^{\mathrm{R23}}$, leading to a similar dynamic as in Figure 4.4b, where both possible Néel states seem to alternately appear and vanish. This can be observed in Figure 4.4c, where this alternating behavior coincides with the measured autocorrelation.

$\hat{H}_j^{\mathrm{R23}}$ is non-hermitian, which causes the time evolution governed by it to be non-unitary. While strong fluctuations of the autocorrelation in such non-unitary evolutions do not generally have the same significance as they do in cases like Section 4.1.3, they at least support the intuitive impression of two conflicting states, fighting over presence.
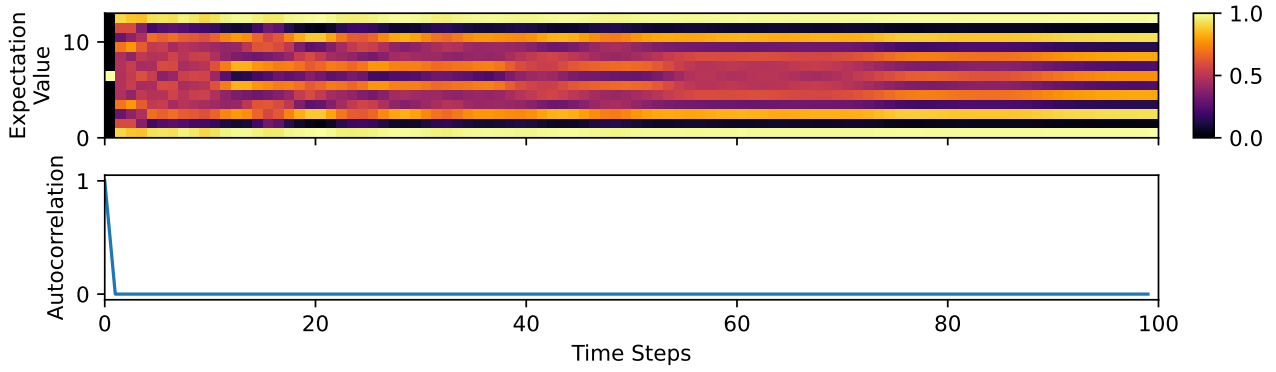
(a) Initial state: $|0\rangle^{\otimes 6} \otimes |1\rangle \otimes |0\rangle^{\otimes 6}$ Boundary conditions: closed
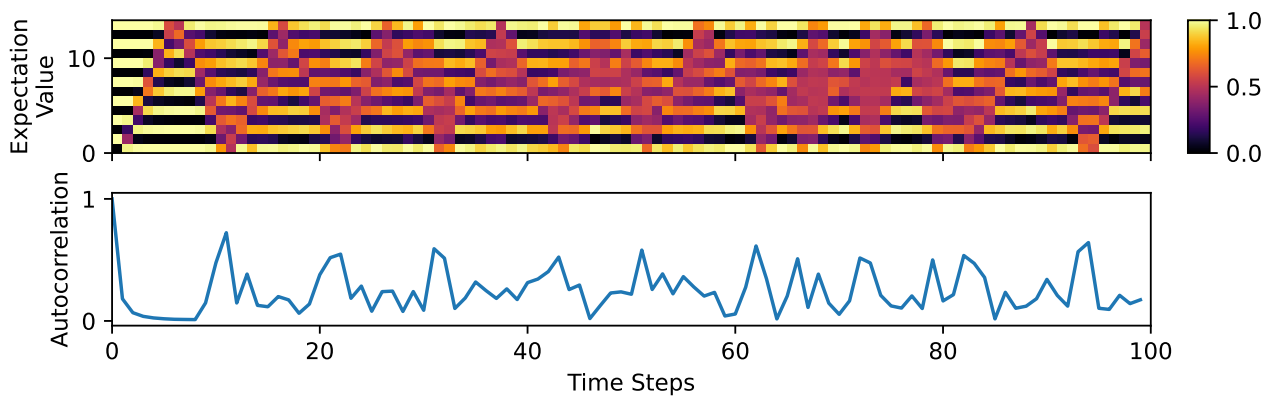
(b) Initial state: $|01010101010101\rangle$ Boundary conditions: closed
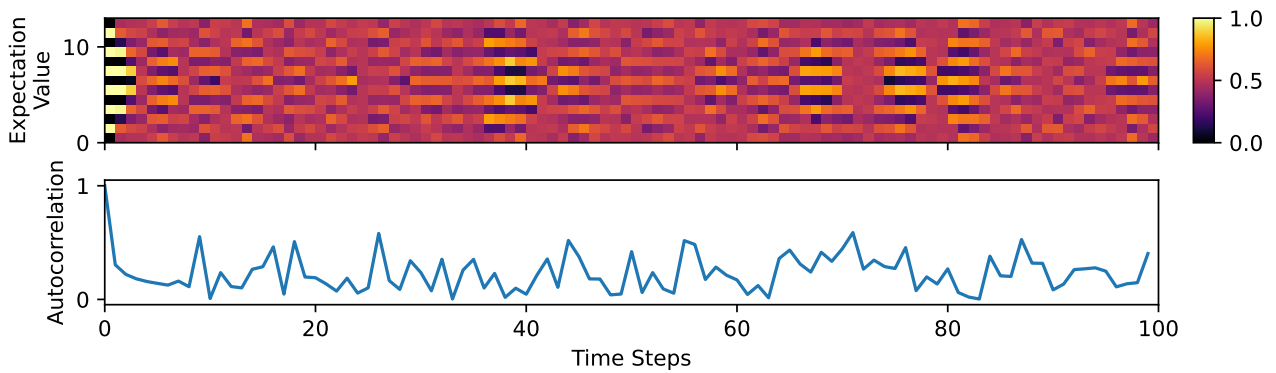
(c) Initial state: $|0101010101010\rangle$ Boundary conditions: periodic

Figure 4.4 Time evolution of the rule 23 QCA for different initial states and boundary conditions. Autocorrelation is calculated as: $\left| \langle\psi|_0 \; |\psi\rangle_t \right|$.
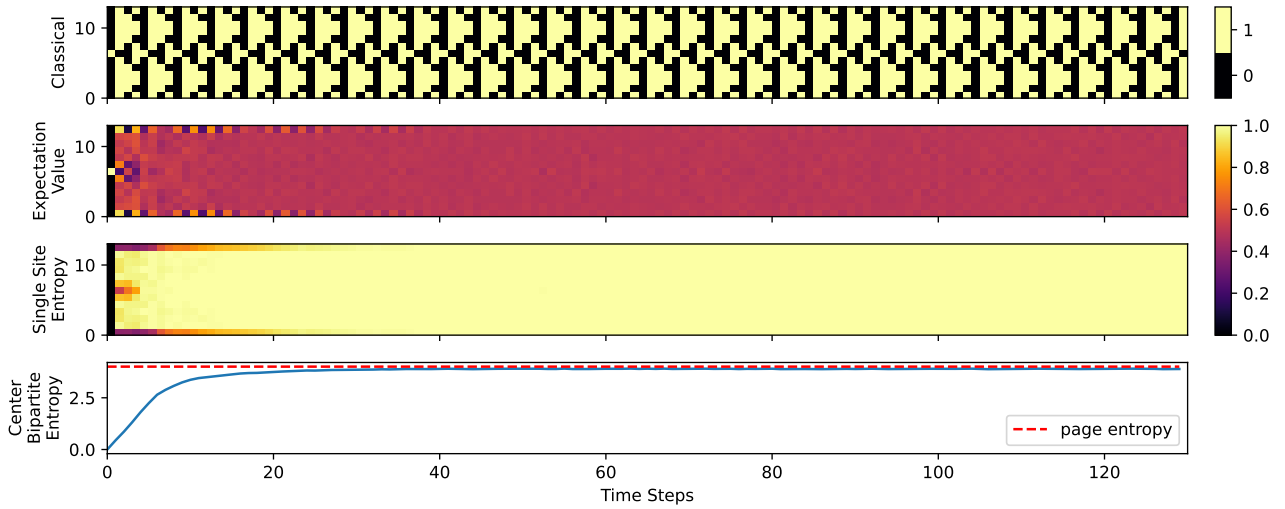
Figure 4.5 Time evolution of the rule 150 QCA with initial state $|0\rangle^{\otimes 6} \otimes |1\rangle \otimes |0\rangle^{\otimes 6}$

4.2.2 Ergodicity in rule 147

$$\hat{H}_j^{R147} = \sigma_j^x \left(n_{j-1}^{|1\rangle} n_{j+1}^{|0\rangle} + n_{j-1}^{|0\rangle} n_{j+1}^{|1\rangle} + n_{j-1}^{|0\rangle} n_{j+1}^{|0\rangle} \right) \tag{4.5}$$

A quantum system is ergodic if its time evolution explores the complete Hilbert space after a sufficiently long time [Pal82]. Ergodic systems are characterized by their thermalization behavior over time, a process where the values of macroscopic quantities converge to stationary values resembling those of a random state [RDO08]. One such quantity is the expectation value of a cell to be in state $|1\rangle$, which trivially equals $\frac{1}{2}$ for random states. Another quantity is the entanglement entropy of a system, which measures the entanglement between the two parts of a bipartition of the complete system. One common bipartition is to split the system in the middle into two parts of the same size. Measuring the entanglement between the two halves results in the center bipartite entropy, which in ergodic systems with L cells converges to the page-entropy value [Pag93]:

$$\frac{L * \log(2) - 1}{2} \tag{4.6}$$

Another possible bipartition is to measure the entanglement between one cell and the rest of the system, the single site entropy. Given a cell j, it is practical to calculate this value as the Von Neumann Entropy $S(\rho_j)$ of the reduced density matrix ρ_j of cell j, resulting from a partial trace over the rest of the system [NC10]:

$$\rho_j = Tr_{\text{rest}} \left(|\psi\rangle \langle \psi| \right) \tag{4.7}$$

$$S(\rho) = -Tr \left(\rho_j \log \left(\rho_j \right) \right) \tag{4.8}$$

For the case of spin-$\frac{1}{2}$ systems, this value lies between 0 and $\log(2)$ [NC10]. Dividing by $\log(2)$ results in a value between 0 and 1, where 0 means no entanglement and 1 means maximal entanglement to the rest of the system. For a random state, the single site entropy is expected to be close to its maximal value [Sen96]. To summarize, states in an ergodic system will thermalize over time, apparent by values like the expectation values of cells to be in state $|1\rangle$, the center bipartite entropy, and the single site entropies converging to values resembling those of random states.

Figure 4.5 shows a plot of the time evolution of the rule 147 QCA undergoing thermalization. Thus, the system is most likely ergodic. Unfortunately, this visual inspection still can not give a definite answer to whether or not a system is completely ergodic. Figure B.1 in Appendix B shows a plot of the rule 147 QCA with periodic instead of closed boundary conditions, which shows the same signs of ergodicity. However, with those modified boundary conditions, the state $|1\rangle^{\otimes L}$, where L is the number of cells, is now an eigenstate of $\hat{H}_j^{R147}$. This

(a) $|\psi\rangle_0 = |\Psi \otimes 0110 \otimes \Psi\rangle$

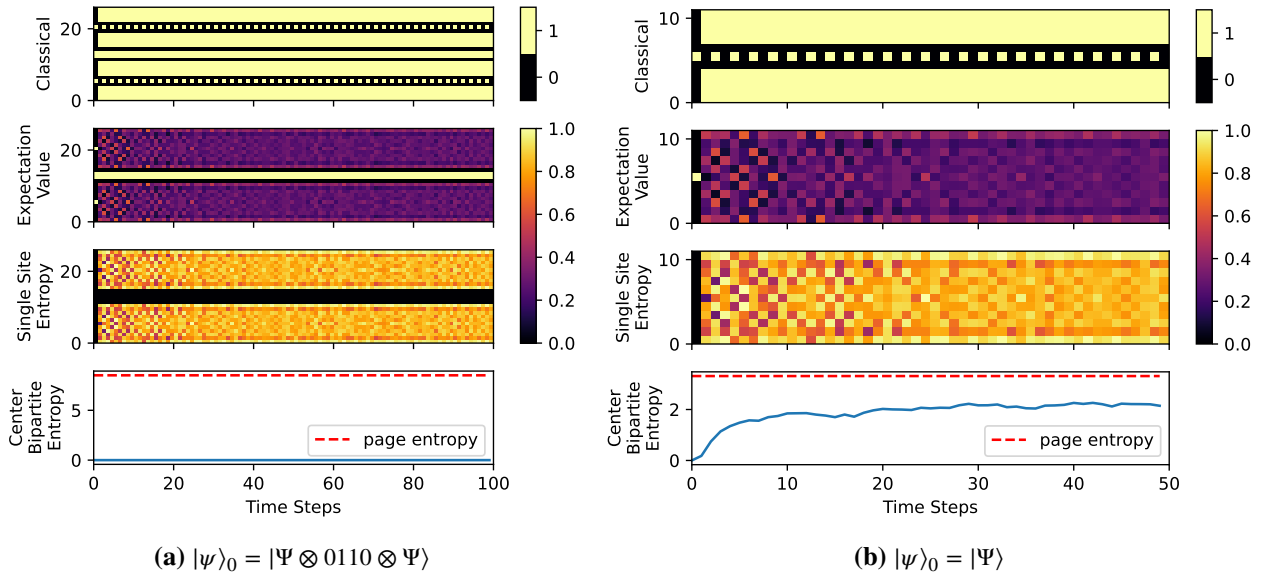(b) $|\psi\rangle_0 = |\Psi\rangle$

Figure 4.6 Comparison of time evolutions of the rule 201 elementary CA for different initial states. $|\Psi\rangle = |00000100000\rangle$.

state would therefore stay constant under the action of $\hat{H}_j^{R147}$ and never explore other parts of the Hilbert space, leading to a breaking of ergodicity. Nevertheless, the plot does not give this fact away and makes one believe the system is fully ergodic.

Even though it can be hard to prove ergodicity in general, there are definite signs of ergodicity breaking. In the case of the rule 147 QCA with periodic boundary conditions, one such sign is the splitting of the Hilbert space into disconnected sectors. The name of this phenomenon is Hilbert space fragmentation.

4.2.3 Hilbert space fragmentation in rule 201

$$\hat{H}_j^{R201} = \sigma_j^x \left(n_{j-1}^{|0\rangle} n_{j+1}^{|0\rangle} \right) \tag{4.9}$$

The rule 201 QCA is also known as the PXP-model, a well-studied quantum system [Tur+18; IV20]. Among the model's distinguishing features are its breaking of ergodicity from Hilbert space fragmentation and quantum many-body scars [Sal+20]. Hilbert space fragmentation refers to a situation where the complete Hilbert space $\mathcal{H}$ is broken apart into dynamically disconnected Krylov spaces [MBR22]:

$$\mathcal{H} = \oplus_j \mathcal{K}_j \qquad \mathcal{K}_j = \text{span} \left\{ |\psi_j\rangle, \hat{H} |\psi_j\rangle, \hat{H}^2 |\psi_j\rangle, \dots \right\} \tag{4.10}$$

To get meaningful results from computing the Hilbert space fragments of a system, the $|\psi_j\rangle$'s in Equation (4.10) should be chosen such that the subspaces $\mathcal{K}_j$ are distinct [MBR22], meaning that no two $|\psi_j\rangle$'s should be chosen from the same Hilbert space fragment.

Choosing the $|\psi_j\rangle$'s as product states is a typical choice in general, as well as specifically for the PXP-model [MBR22; Tur+18]. When doing so, the reason for the Hilbert space fragmentation in rule 201 is revealed to be the existence of frozen states [Sal+20], which are states where some cells stay constant, even after arbitrary time lengths. Cell configurations where two or more adjacent cells are in state $|1\rangle$ will remain so under the action of $\hat{H}_j^{R201}$, thus such a state is frozen. Additionally, the immediate neighbor cells of such a frozen cell chain will also never change, due to having at least one frozen neighbor in state $|1\rangle$. The length and position of a frozen cell chain can therefore not change. New frozen cell chains can also not emerge from nothing, as a time reversal of such an event would be equivalent to breaking up a frozen cell chain, which is impossible. Finally, the Hilbert space fragment of non-frozen states is in itself ergodic, meaning that every state from this segment explores the complete fragment during a time evolution, preventing further fragmentation [Tur+18].

To summarize, a time evolution from an initial state will never leave its own fragment, as parts of the Hilbert space with a different number or position of frozen cell chains remain inaccessible, regardless of how long the

time evolution goes on. This results in a fragmentation of the Hilbert space where each fragment can be labeled by the position and length of their respective frozen cell chains. The number of Hilbert space fragments of the rule 201 QCA in the $\{|0\rangle, |1\rangle\}$-basis grows exponentially with the number of cells, which classifies the QCA as a strongly fragmented system, breaking ergodicity [Sal+20]. This fact becomes visible in Figure 4.6 where a time evolution of the rule 201 QCA is shown for two different system sizes and initial states. The plots show none of the signs of thermalization discussed in Section 4.2.2, as neither the expectation value of cell states, the single site entropy, nor the center bipartite entropy converge to values resembling those of a random state. Figure B.3 in Appendix B shows longer versions of Figure 4.6b, where even after $2 \cdot 10^{12}$ time steps no sign of thermalization is showing. This reinforces the fact that the rule 201 QCA is not ergodic.

For the case of the rule 201 QCA, frozen cell chains are a very visible phenomenon, lending themselves to some easy intuition to be gained by observing their time evolution. The range of $\hat{H}_j^{\text{R201}}$ is 1, while the length of a frozen cell chain is at least 2, so no interaction from one side of a frozen cell chain to the other can occur. A frozen cell chain therefore splits the cell lattice into two parts that can not interact. This leads to a situation where both parts behave like independent closed systems with closed boundary conditions. This situation can be observed in Figure 4.6a, where two adjacent cells in state $|1\rangle$ split the system in the middle. Both of the isolated segments show the same time evolution as the independently simulated system shown in Figure 4.6b. This isolating behavior also explains the fact that the center bipartite entropy in Figure 4.6a is constant, as no entanglement between the isolated systems can form.

Another interesting observation can be made when inspecting how the different terms from Equation (3.8) interact with the states of different Hilbert space fragments. Focusing only on the Hilbert space fragment without frozen states for now, spanned by all product states without two or more adjacent cells in $|1\rangle$ state, the set of cell triplets found in such a product state is

$$\{|000\rangle, |001\rangle, |010\rangle, |100\rangle, |101\rangle\} \tag{4.11}$$

Looking at the NRT-decomposition of rule 201, one can identify the parts of the rule where these cell triplets act as initial states and ignore them (crossed out):

activators	$n_{j-1}^{|1\rangle} n_{j+1}^{|1\rangle}$		$n_{j-1}^{|1\rangle} n_{j+1}^{|0\rangle}$		$n_{j-1}^{|0\rangle} n_{j+1}^{|1\rangle}$		$n_{j-1}^{|0\rangle} n_{j+1}^{|0\rangle}$	
b	**1** ☐ **1**		**1** ☐ **0**		**0** ☐ **1**		**0** ☐ **0**	
time step	1 1 1 ↓ 1 1 1	1 0 1 ↓ 1 0 1	1 1 0 ↓ 1 1 0	1 0 0 ↓ 1 0 0	0 1 1 ↓ 0 1 1	0 0 1 ↓ 0 0 1	0 1 0 ↓ 0 0 0	0 0 0 ↓ 0 1 0
NRT$(101, b)$	$(\{0, 1\}, 0)$		$(\{0, 1\}, 0)$		$(\{0, 1\}, 0)$		$(0, 1)$	
behavior	{set to 0, no change}						bit flip	
type	{peripheral, reversible}						reversible	

$$\tag{4.12}$$

As a consequence, additional degrees of freedom are added for choosing the corresponding operators $\hat{S}_j$. Any of the $\hat{S}_j$'s corresponding to one of the activation terms $\left\{ n_{j-1}^{|1\rangle} n_{j+1}^{|1\rangle}, n_{j-1}^{|1\rangle} n_{j+1}^{|0\rangle}, n_{j-1}^{|0\rangle} n_{j+1}^{|1\rangle} \right\}$ can either be set to $\hat{S}_j^{\text{no change}}$ or $\hat{S}_j^{\text{set to 0}}$ without changing the behavior of any non-frozen state, as it is only relevant that $|0\rangle$ is mapped to $|0\rangle$, not how $|1\rangle$ is mapped. Thus, there are other rules for QCAs where an initial state from the Hilbert space fragment of non-frozen states will show the same time evolution to the rule 201 QCA.

The unabbreviated version of Equation (4.9) is given by

$$\hat{H}_j^{\text{R201}} = \hat{S}_j^{\text{bit flip}} \left(n_{j-1}^{|0\rangle} n_{j+1}^{|0\rangle} \right) + \hat{S}_j^{\text{no change}} \left(n_{j-1}^{|0\rangle} n_{j+1}^{|1\rangle} \right) + \hat{S}_j^{\text{no change}} \left(n_{j-1}^{|1\rangle} n_{j+1}^{|0\rangle} \right) + \hat{S}_j^{\text{no change}} \left(n_{j-1}^{|1\rangle} n_{j+1}^{|1\rangle} \right) \tag{4.13}$$

Any of the $\hat{S}_j^{\text{no change}}$ operators can now either be exchanged with the $\hat{S}_j^{\text{set to 0}}$ operator or kept constant, leading to $2^3 = 8$ rules matching the NRT-decomposition from Equation (4.12). As expected, the time evolutions for

all of the rules that can result from this process are identical to the time evolution of the rule 201 QCA, if the initial state was taken from the Hilbert space fragment of non-frozen states. Plots for all 8 rules are shown in Figures B.4 and B.5 in Appendix B.

Notably, all of the 8 QCAs except for the one corresponding to rule 201 are governed by a non-hermitian Hamiltonian, as their NRT-decompositions include peripheral terms. Nevertheless, because of their equivalence inside of the Hilbert space fragment of non-frozen states, they perform a unitary time evolution for all states in this fragment.

5 Outlook

This thesis demonstrated potential methods for developing a quantum analogue to classical elementary cellular automata CAs. Moreover, it established that valuable insights and intuitive understanding can be derived from comparing these two classes of systems. Nevertheless, while researching background knowledge and examining newly created plots, I formed many new ideas that could not be explored further due to time limitations. While I intend to expand upon these ideas in future work, they are presented here with the hope of inspiring subsequent research by others.

5.1 Non-unitary dynamics

The fact that some of the QCAs resulting from the methods shown in this thesis are non-unitary is troublesome, as such systems can not be physical if they are also demanded to be closed. There are at least two possible solutions for this problem.

The section on time evolutions (cf. Section 3.2) touched upon the fact that non-unitary systems can be thought of as the result of viewing a partial trace of a larger system, in turn undergoing a unitary time evolution. There might therefore be a way to construct such a larger, closed, and unitary system where a suitable partial trace reveals the desired non-unitary time evolution. A promising approach could be using a system-environment model, as described in [WBC15], where the reduced, non-unitary dynamic must first be modeled as a quantum channel in Kraus representation before being embedded into the larger system. If successful, one could compare the time evolution inside of the reduced system to the one outside, speculating to find a kind of "inverse" time evolution.

Another approach is to use quantum measurements and the resulting collapse of the wave function as a tool to achieve arbitrary non-unitary rules, as explained in [TU05]. The quantum wave collapse is non-unitary in nature [NC10], so if a system could be brought into a state where at least one possible measurement outcome would collapse the system into a state equivalent to one resulting from the desired non-unitary evolution, there is a chance that the system will have performed the desired time evolution after measurement. This process is made possible by introducing ancilla Qubits to help simulate an arbitrary quantum measurement. If the measurement outcome does not correspond to the desired behavior, the experiment could be restarted.

5.2 Alternative operators for peripheral rules

The two operator sets presented in Section 3.4 are not an exhaustive list. There are most likely other operators with better convergence behavior or less drastic scaling issues. It could also prove successful to find operators that only initially show the desired behavior while diverging to a different dynamic at later times. During testing, one of my approaches was to use the operators from Section 3.4.2 in the limit of $t \to \infty$ in turn as operators governing a time evolution:

$$\hat{S}''_{|0\rangle} = |0\rangle \langle 0| + |0\rangle \langle 1| \qquad \hat{S}''_{|1\rangle} = |1\rangle \langle 0| + |1\rangle \langle 1| \tag{5.1}$$

While a time evolution governed by these operators does not show the same convergence to the desired basis state as the other two presented solutions, they initially show a similar behavior, while producing much fewer scaling issues.

A Equations

A.1 Time evolution of arbitrary state governed by the projection operator set (cf. Section 3.4.2)

$$
\begin{aligned}
|\psi\rangle_{|0\rangle}(t) &= \left(I + \left(e^{-t} - 1\right) i\hat{H}_{|0\rangle}\right)|\psi\rangle \\
&= |\psi\rangle + \left(e^{-t} - 1\right) i\hat{H}_{|0\rangle}|\psi\rangle \\
&= \alpha|0\rangle + \beta|1\rangle - \beta\left(e^{-t} - 1\right)(|0\rangle - |1\rangle) \\
&= \left(\alpha - \beta e^{-t} + \beta\right)|0\rangle + \beta e^{-t}|1\rangle \\
&\xrightarrow{normalize} \frac{\left(\alpha - \beta e^{-t} + \beta\right)|0\rangle + \beta e^{-t}|1\rangle}{\sqrt{|\alpha - \beta e^{-t} + \beta|^2 + |\beta e^{-t}|^2}}
\end{aligned}
\tag{A.1}
$$

$$
\begin{aligned}
|\psi\rangle_{|1\rangle}(t) &= \left(I + \left(e^{-t} - 1\right) i\hat{H}_{|1\rangle}\right)|\psi\rangle \\
&= |\psi\rangle + \left(e^{-t} - 1\right) i\hat{H}_{|1\rangle}|\psi\rangle \\
&= \alpha|0\rangle + \beta|1\rangle + \alpha\left(e^{-t} - 1\right)(|0\rangle - |1\rangle) \\
&= \alpha e^{-t}|0\rangle + \left(\beta - \alpha e^{-t} + \alpha\right)|1\rangle \\
&\xrightarrow{normalize} \frac{\alpha e^{-t}|0\rangle + \left(\beta - \alpha e^{-t} + \alpha\right)|1\rangle}{\sqrt{|\alpha e^{-t}|^2 + |\beta - \alpha e^{-t} + \alpha|^2}}
\end{aligned}
\tag{A.2}
$$

$$
\begin{aligned}
Pr\left[|\psi\rangle_{|0\rangle}(t) = |0\rangle\right] &= \left|\langle 0|\left(\frac{\left(\alpha - \beta e^{-t} + \beta\right)|0\rangle + \beta e^{-t}|1\rangle}{\sqrt{|\alpha - \beta e^{-t} + \beta|^2 + |\beta e^{-t}|^2}}\right)\right|^2 \\
&= \left|\frac{\alpha - \beta e^{-t} + \beta}{\sqrt{|\alpha - \beta e^{-t} + \beta|^2 + |\beta e^{-t}|^2}}\right|^2 \\
&= \frac{|\alpha - \beta e^{-t} + \beta|^2}{|\alpha - \beta e^{-t} + \beta|^2 + |\beta e^{-t}|^2}
\end{aligned}
\tag{A.3}
$$

$$
\begin{aligned}
Pr\left[|\psi\rangle_{|0\rangle}(t) = |1\rangle\right] &= \left|\langle 1|\left(\frac{\left(\alpha - \beta e^{-t} + \beta\right)|0\rangle + \beta e^{-t}|1\rangle}{\sqrt{|\alpha - \beta e^{-t} + \beta|^2 + |\beta e^{-t}|^2}}\right)\right|^2 \\
&= \left|\frac{\beta e^{-t}}{\sqrt{|\alpha - \beta e^{-t} + \beta|^2 + |\beta e^{-t}|^2}}\right|^2 \\
&= \frac{|\beta e^{-t}|^2}{|\alpha - \beta e^{-t} + \beta|^2 + |\beta e^{-t}|^2}
\end{aligned}
\tag{A.4}
$$

$$Pr\left[|\psi\rangle_{|1\rangle}(t) = |0\rangle\right] = \left|\langle 0|\left(\frac{\alpha e^{-t}|0\rangle + \left(\beta - \alpha e^{-t} + \alpha\right)|1\rangle}{\sqrt{|\alpha e^{-t}|^2 + |\beta - \alpha e^{-t} + \alpha|^2}}\right)\right|^2$$

$$= \left|\frac{\alpha e^{-t}}{\sqrt{|\alpha e^{-t}|^2 + |\beta - \alpha e^{-t} + \alpha|^2}}\right|^2 \tag{A.5}$$

$$= \frac{|\alpha e^{-t}|^2}{|\alpha e^{-t}|^2 + |\beta - \alpha e^{-t} + \alpha|^2}$$

$$Pr\left[|\psi\rangle_{|1\rangle}(t) = |1\rangle\right] = \left|\langle 1|\left(\frac{\alpha e^{-t}|0\rangle + \left(\beta - \alpha e^{-t} + \alpha\right)|1\rangle}{\sqrt{|\alpha e^{-t}|^2 + |\beta - \alpha e^{-t} + \alpha|^2}}\right)\right|^2$$

$$= \left|\frac{\beta - \alpha e^{-t} + \alpha}{\sqrt{|\alpha e^{-t}|^2 + |\beta - \alpha e^{-t} + \alpha|^2}}\right|^2 \tag{A.6}$$

$$= \frac{|\beta - \alpha e^{-t} + \alpha|^2}{|\alpha e^{-t}|^2 + |\beta - \alpha e^{-t} + \alpha|^2}$$

A.2 Singular values of time evolution operators governed by the projection operator set (cf. Section 3.4.2)

Similar to the case of operator set 1, both operators have the same singular values, so it again suffices to calculate the singular values of a generic $\hat{U}'_{|k\rangle} \in \left\{\hat{U}'_{|0\rangle}, \hat{U}'_{|0\rangle}\right\}$:

$$\det\left(\hat{U}'^{\dagger}_{|k\rangle}\hat{U}'_{|k\rangle} - \lambda I\right) = \lambda^2 - \lambda\left(2 - 2e^{-t} + 2e^{-2t}\right) + e^{-2t} \stackrel{!}{=} 0 \tag{A.7}$$

$$\lambda_{1,2}(t) = 1 - e^{-t} + e^{-2t} \pm \sqrt{\left(1 - e^{-t} + e^{-2t}\right)^2 - e^{-2t}} \tag{A.8}$$

The singular values $s_{1,2}(t)$ are then the square roots of $\lambda_{1,2}$

$$s_{1,2}(t) = \sqrt{1 - e^{-t} + e^{-2t} \pm \sqrt{\left(1 - e^{-t} + e^{-2t}\right)^2 - e^{-2t}}} \tag{A.9}$$

Viewing the limit of $t \to \infty$

$$\lim_{t\to\infty} s_1(t) = \sqrt{2} \qquad\qquad \lim_{t\to\infty} s_2(t) = 0 \tag{A.10}$$
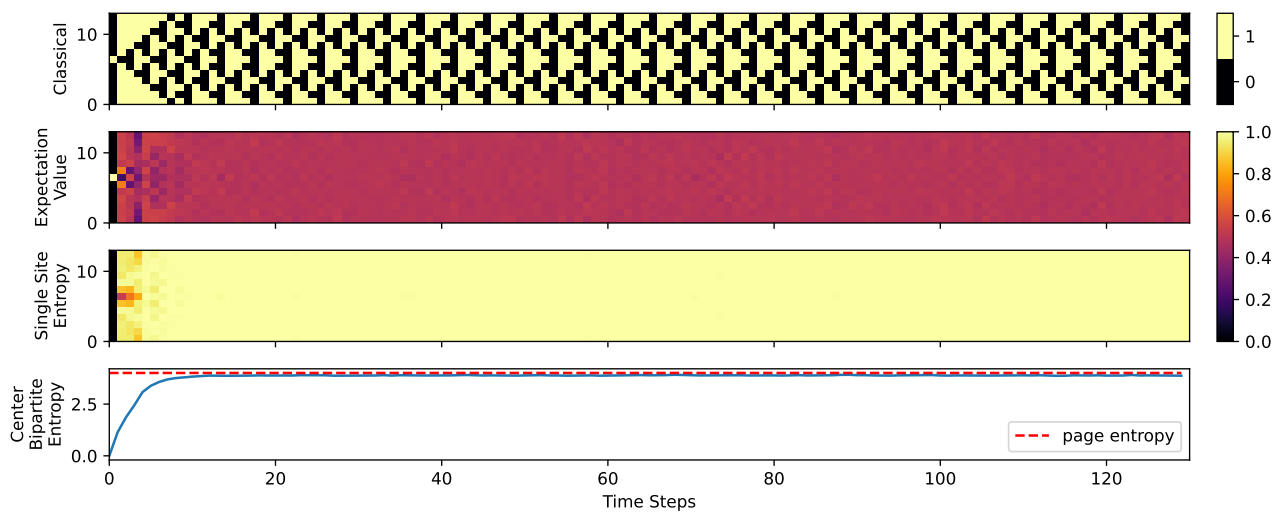
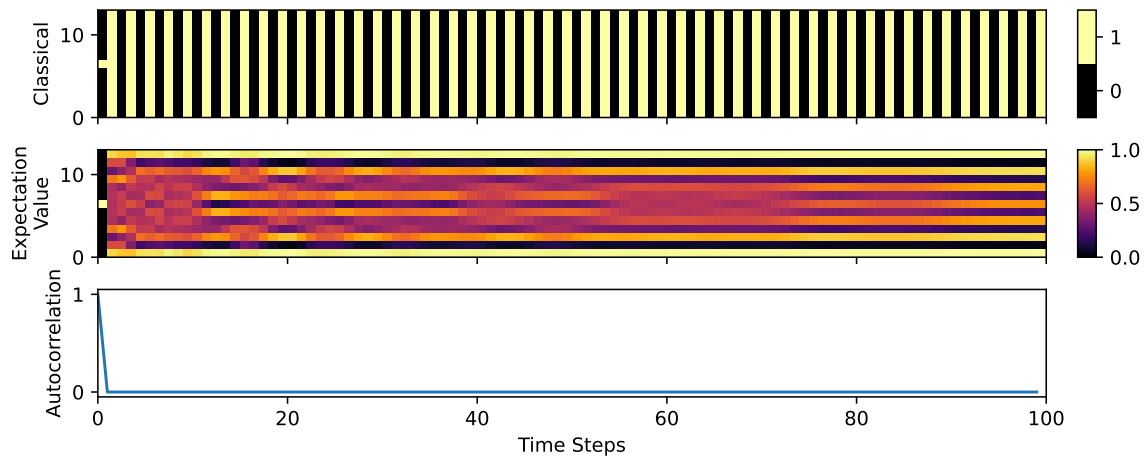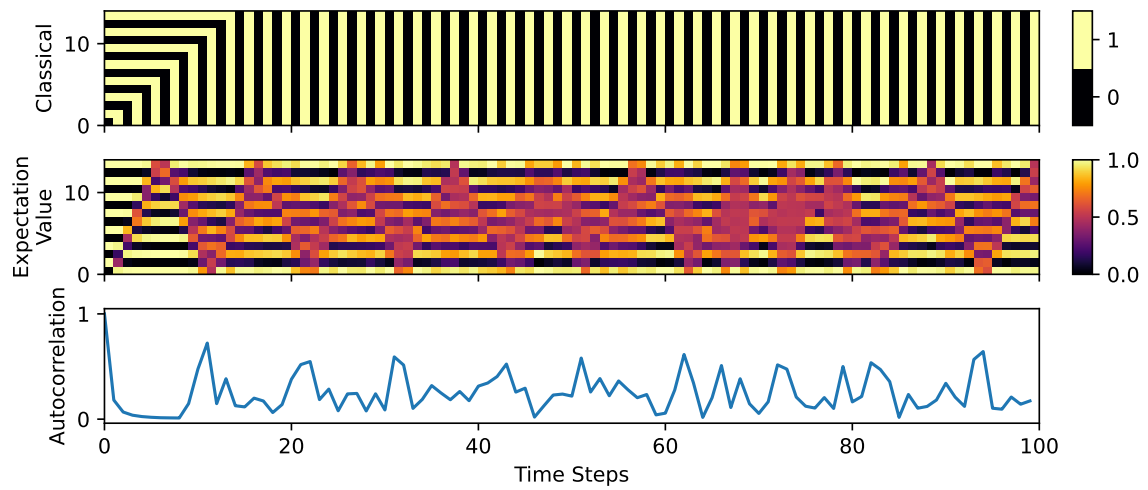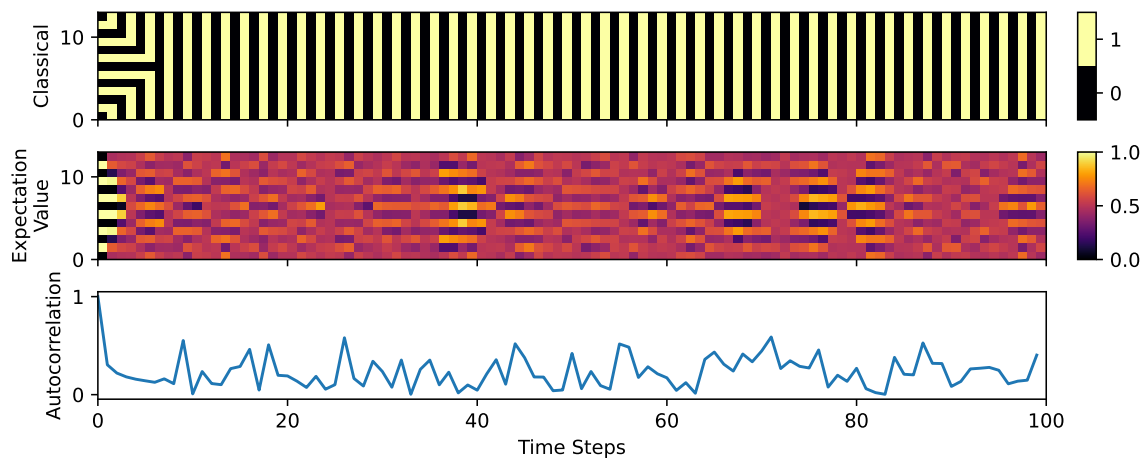aligns with expectations.

B Figures

Figure B.1 Time evolution of the rule 150 QCA with initial state $|0\rangle^{\otimes 6} \otimes |1\rangle \otimes |0\rangle^{\otimes 6}$ with periodic boundary conditions

(a) Initial state: $|0\rangle^{\otimes 6} \otimes |1\rangle \otimes |0\rangle^{\otimes 6}$ Boundary conditions: closed

(b) Initial state: $|01010101010101\rangle$ Boundary conditions: closed

(c) Initial state: $|0101010101010\rangle$ Boundary conditions: periodic

Figure B.2 Time evolution of the rule 23 QCA for different initial states and boundary conditions. Autocorrelation is calculated as: $\left|\langle\psi|_0\ |\psi\rangle_t\right|$.
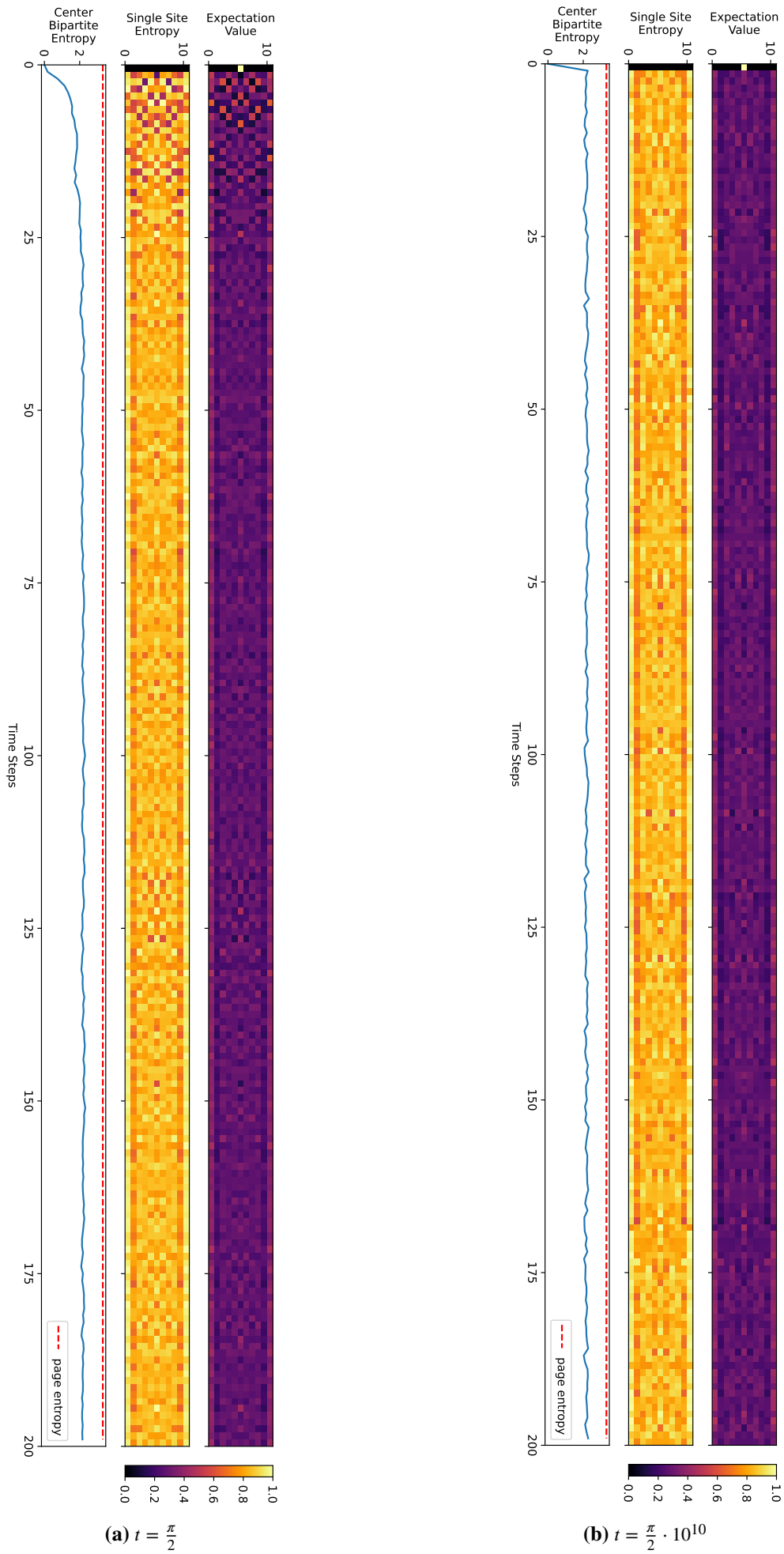
Figure B.3 Plots of the time evolution of the rule 201 QCA showing the expectation value of cell states, single site entropy, and center bipartite entropy for different time step sizes t
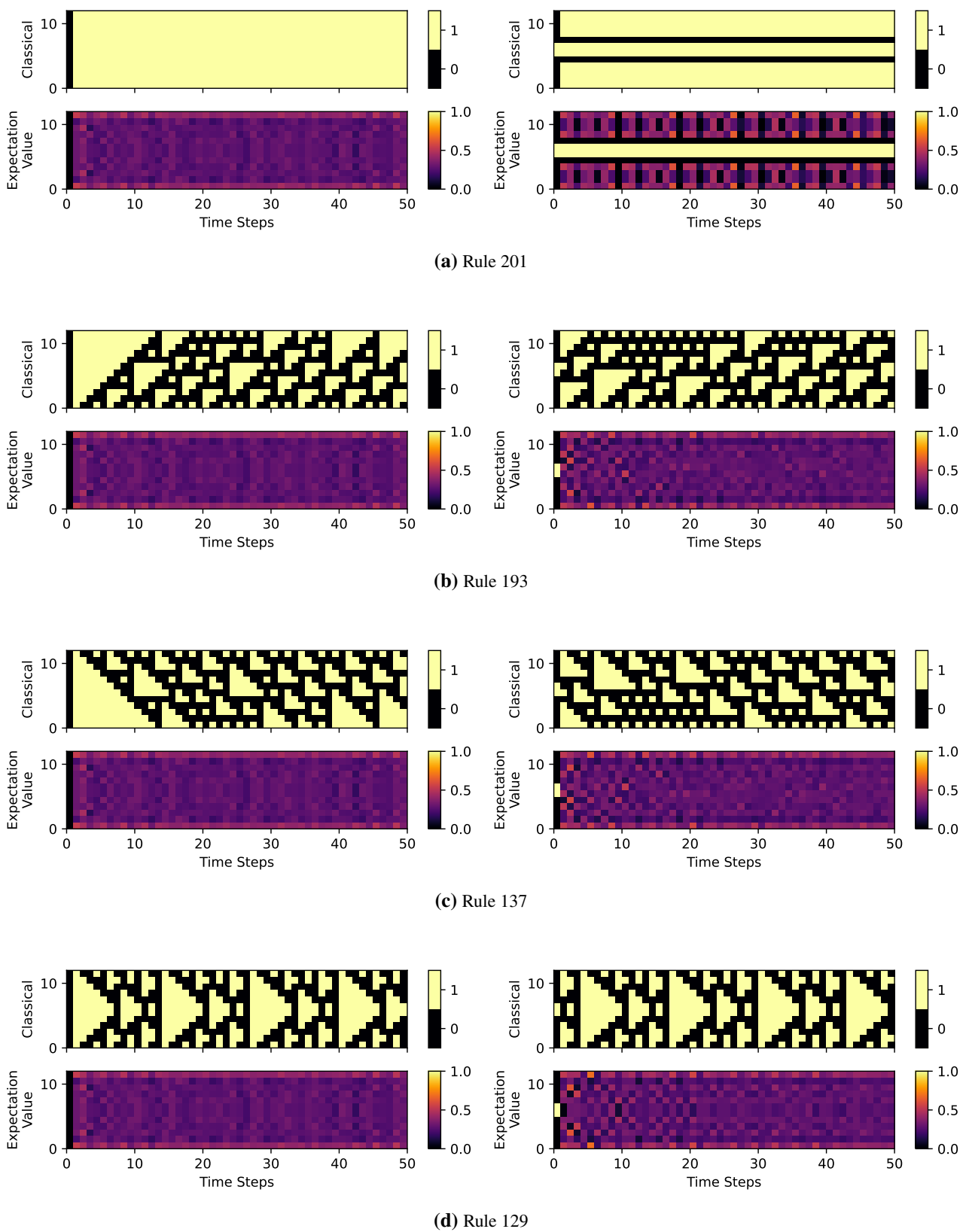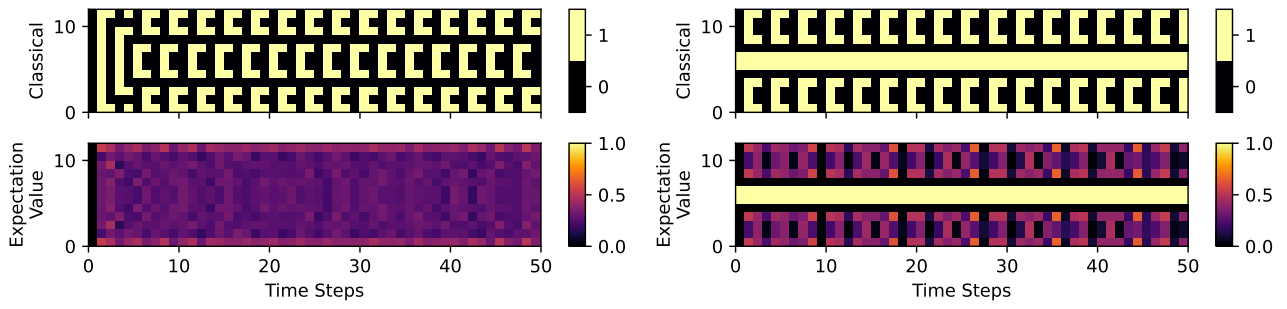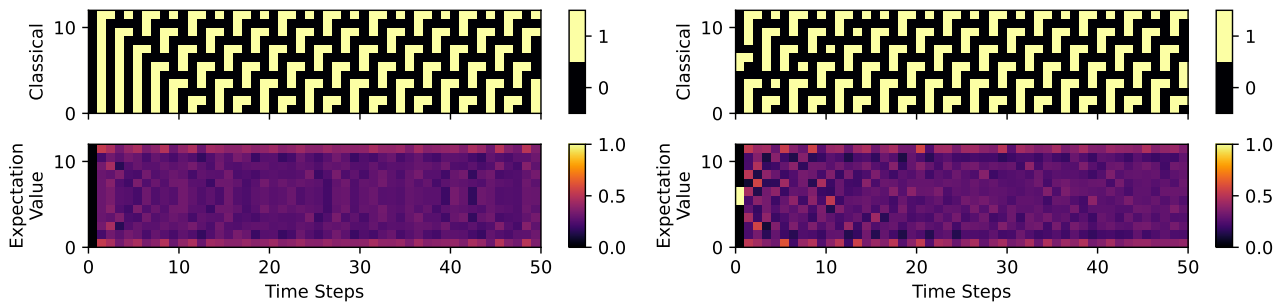
(a) Rule 201

(b) Rule 193

(c) Rule 137

(d) Rule 129

Figure B.4 Classical and quantum time evolutions of different rules. The left side shows evolutions for initial state $|0\rangle^{\otimes 8}$, the right side for $|0\rangle^{\otimes 5} \otimes |11\rangle \otimes |0\rangle^{\otimes 5}$
Part 1

B Figures

(a) Rule 73

(b) Rule 65

(c) Rule 9

(d) Rule 1

Figure B.5 Classical and quantum time evolutions of different rules. The left side shows evolutions for initial state $|0\rangle^{\otimes 8}$, the right side for $|0\rangle^{\otimes 5} \otimes |11\rangle \otimes |0\rangle^{\otimes 5}$
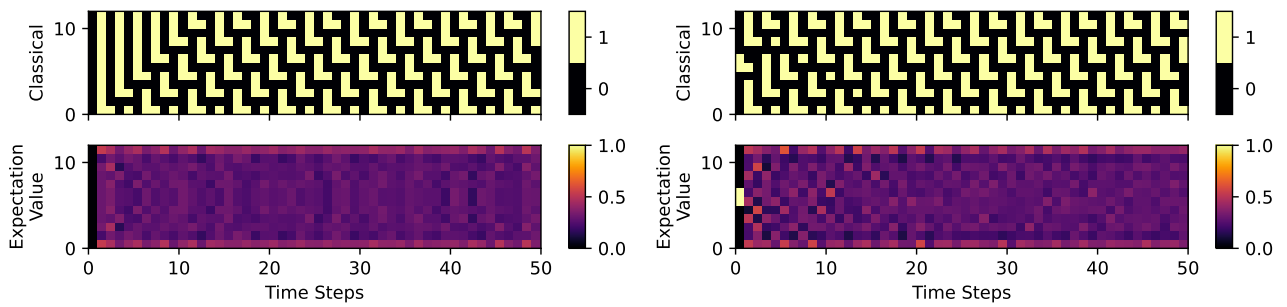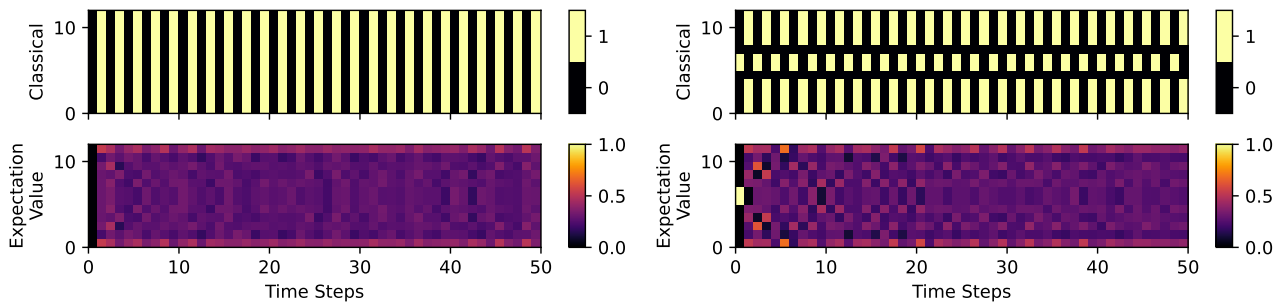
Part 2

Glossary

CA cellular automaton.

NRT neighborhood rule tuple.

PQCA partitioned quantum cellular automaton.

QCA quantum cellular automaton.

Bibliography

[Arr19]   P. Arrighi. "An overview of quantum cellular automata". en. In: *Natural Computing* 18.4 (2019-12), pp. 885–899. DOI: `10.1007/s11047-019-09762-6`.

[BCG04]   Elwyn R. Berlekamp, John H. Conway, and Richard K. Guy. *Winning Ways for Your Mathematical Plays, Volume 4*. 2nd ed. New York: A K Peters/CRC Press, 2004-03. ISBN: 978-0-429-48730-9. DOI: `10.1201/9780429487309`.

[BCM12]   D. Bleh, T. Calarco, and S. Montangero. "Quantum Game of Life". en. In: *Europhysics Letters* 97.2 (2012-01), p. 20012. DOI: `10.1209/0295-5075/97/20012`.

[BL57]   P. Bocchieri and A. Loinger. "Quantum Recurrence Theorem". In: *Physical Review* 107.2 (1957-07), pp. 337–338. DOI: `10.1103/PhysRev.107.337`.

[Coo04]   Matthew Cook. "Universality in Elementary Cellular Automata". In: *Complex Systems* 1 (2004-03). DOI: `10.25088/ComplexSystems.15.1.1`.

[Dec24]   Benjamin Decker. *QuantumGameOfLife.jl*. Version 1.0.0. 2024-09. URL: `https://github.com/BenjaminDecker/QuantumGameOfLife.jl`.

[Dec23]   Florian Felix Benjamin Decker. *Implementation of a Classical Simulation of Quantum Cellular Automata on 1-D Lattices and using it to Improve the Tensor Network Algorithm TDVP*. 2023. URL: `https://mediatum.ub.tum.de/1707205`.

[Far20]   Terry Farrelly. "A review of Quantum Cellular Automata". en-GB. In: *Quantum* 4 (2020-11), p. 368. DOI: `10.22331/q-2020-11-30-368`.

[FWS22a]   Matthew Fishman, Steven R. White, and E. Miles Stoudenmire. "Codebase release 0.3 for ITensor". In: *SciPost Phys. Codebases* (2022), 4–r0.3. DOI: `10.21468/SciPostPhysCodeb.4-r0.3`.

[FWS22b]   Matthew Fishman, Steven R. White, and E. Miles Stoudenmire. "The ITensor Software Library for Tensor Network Calculations". In: *SciPost Phys. Codebases* (2022), p. 4. DOI: `10.21468/SciPostPhysCodeb.4`.

[Gro+12]   D. Gross et al. "Index Theory of One Dimensional Quantum Walks and Cellular Automata". en. In: *Communications in Mathematical Physics* 310.2 (2012-03), pp. 419–454. DOI: `10.1007/s00220-012-1423-1`.

[Hae+11]   Jutho Haegeman et al. "Time-Dependent Variational Principle for Quantum Lattices". In: *Physical Review Letters* 107.7 (2011-08), p. 070601. DOI: `10.1103/PhysRevLett.107.070601`.

[Hae+16]   Jutho Haegeman et al. "Unifying time evolution and optimization with matrix product states". In: *Physical Review B* 94.16 (2016-10), p. 165116. DOI: `10.1103/PhysRevB.94.165116`.

[IV20]   Thomas Iadecola and Sagar Vijay. "Nonergodic quantum dynamics from deformations of classical cellular automata". In: *Physical Review B* 102.18 (2020-11), p. 180302. DOI: `10.1103/PhysRevB.102.180302`.

[ICS15]   Eugene M Izhikevich, John H Conway, and Anil Seth. "Game of life". In: *Scholarpedia* 10.6 (2015), p. 1816.

[LP+90]   Wentian Li, Norman Packard, et al. "The structure of the elementary cellular automata rule space". In: *Complex systems* 4.3 (1990), pp. 281–297. URL: `https://www.complex-systems.com/abstracts/v04_i03_a03/`.

[MBR22]   Sanjay Moudgalya, B. Andrei Bernevig, and Nicolas Regnault. "Quantum many-body scars and Hilbert space fragmentation: a review of exact results". en. In: *Reports on Progress in Physics* 85.8 (2022-07), p. 086501. DOI: 10.1088/1361-6633/ac73a0.

[Ney+22]   Peter-Maximilian Ney et al. "Entanglement in the quantum Game of Life". In: *Physical Review A* 105.1 (2022-01), p. 012416. DOI: 10.1103/PhysRevA.105.012416.

[NC10]   Michael A. Nielsen and Isaac L. Chuang. *Quantum Computation and Quantum Information: 10th Anniversary Edition*. en. 2010-12. DOI: 10.1017/CBO9780511976667.

[Pae+19]   Sebastian Paeckel et al. "Time-evolution methods for matrix-product states". In: *Annals of Physics* 411 (2019-12), p. 167998. DOI: 10.1016/j.aop.2019.167998.

[Pag93]   Don N. Page. "Average entropy of a subsystem". In: *Physical Review Letters* 71.9 (1993-08), pp. 1291–1294. DOI: 10.1103/PhysRevLett.71.1291.

[Pal82]   R.G. Palmer. "Broken ergodicity". In: *Advances in Physics* 31.6 (1982-12), pp. 669–735. DOI: 10.1080/00018738200101438.

[Per61]   Ian C. Percival. "Almost Periodicity and the Quantal H Theorem". In: *Journal of Mathematical Physics* 2.2 (1961-03), pp. 235–239. DOI: 10.1063/1.1703705.

[RDO08]   Marcos Rigol, Vanja Dunjko, and Maxim Olshanii. "Thermalization and its mechanism for generic isolated quantum systems". en. In: *Nature* 452.7189 (2008-04), pp. 854–858. DOI: 10.1038/nature06838.

[Sal+20]   Pablo Sala et al. "Ergodicity Breaking Arising from Hilbert Space Fragmentation in Dipole-Conserving Hamiltonians". In: *Physical Review X* 10.1 (2020-02), p. 011047. DOI: 10.1103/PhysRevX.10.011047.

[Sch78]   L. S. Schulman. "Note on the quantum recurrence theorem". In: *Physical Review A* 18.5 (1978-11), pp. 2379–2380. DOI: 10.1103/PhysRevA.18.2379.

[SW04]   B. Schumacher and R. F. Werner. "Reversible quantum cellular automata". In: (2004-05). DOI: 10.48550/arXiv.quant-ph/0405174.

[Sen96]   Siddhartha Sen. "Average Entropy of a Quantum Subsystem". In: *Physical Review Letters* 77.1 (1996-07), pp. 1–3. DOI: 10.1103/PhysRevLett.77.1.

[Sut09]   Klaus Sutner. "Classification of cellular automata". In: *Encyclopedia of Complexity and Systems Science, Part* 3 (2009), pp. 755–768.

[TU05]   Hiroaki Terashima and Masahito Ueda. "Nonunitary quantum circuit". In: *International Journal of Quantum Information* 03.04 (2005-12), pp. 633–647. ISSN: 0219-7499. DOI: 10.1142/S0219749905001456.

[Tur+18]   C. J. Turner et al. "Quantum scarred eigenstates in a Rydberg atom chain: Entanglement, breakdown of thermalization, and stability to perturbations". In: *Physical Review B* 98.15 (2018-10), p. 155134. DOI: 10.1103/PhysRevB.98.155134.

[VPM15]   R. Vasseur, S. A. Parameswaran, and J. E. Moore. "Quantum revivals and many-body localization". In: *Physical Review B* 91.14 (2015-04), p. 140202. DOI: 10.1103/PhysRevB.91.140202.

[Wat95]   J. Watrous. "On one-dimensional quantum cellular automata". In: *Proceedings of IEEE 36th Annual Foundations of Computer Science*. 1995-10, pp. 528–537. DOI: 10.1109/SFCS.1995.492583.

[Wol18]   Stephen Wolfram. *Cellular automata and complexity: collected papers*. crc Press, 2018.

[Wol83]   Stephen Wolfram. "Statistical mechanics of cellular automata". In: *Reviews of Modern Physics* 55.3 (1983-07), pp. 601–644. DOI: 10.1103/RevModPhys.55.601.

[WW17]   Inc. Wolfram Research and Stephen Wolfram. "A New Kind of Science: A 15-Year View". In: *Complex Systems* 26.3 (2017-10), pp. 197–224. DOI: 10.25088/ComplexSystems.26.3.197.

[WBC15]   Christopher J. Wood, Jacob D. Biamonte, and David G. Cory. "Tensor networks and graphical calculus for open quantum systems". In: (2015-05). DOI: 10.48550/arXiv.1111.6950.